

Anisotropic magnetization, specific heat and resistivity of $R\text{Fe}_2\text{Ge}_2$ single crystals

M. A. Avila¹, S. L. Bud'ko¹, P. C. Canfield¹

¹Ames Laboratory and Department of Physics and Astronomy
Iowa State University, Ames, IA 50011

Abstract

We have grown $R\text{Fe}_2\text{Ge}_2$ single crystals for $R = \text{Y}$ and ten members of the lanthanide series (Pr, Nd, Sm, Gd-Tm, Lu) using Sn flux as the solvent. The method yields clean, high quality crystal plates as evidenced by residual resistivities and RRR values in the range of 3-12 $\mu\Omega\text{cm}$ and 20-90 respectively. The crystals are also virtually free of magnetic impurities or secondary phases, allowing the study of the intrinsic anisotropic magnetic behavior of each compound. Characterization was made with X-Ray diffraction, and temperature and field dependent magnetization, specific heat and resistivity. Very strong anisotropies arising mostly from CEF effects were observed for all magnetic rare earths except Gd. Antiferromagnetic ordering occurred at temperatures between 16.5 K (Nd) and 1.1 K (Ho) that roughly scale with the de Gennes factor for the heavy rare earths. For some members there is also a lower temperature transition associated with changes in the magnetic structure. Tm did not order down to 0.4 K, and appears to be a van Vleck paramagnet. All members which ordered above 2 K showed a metamagnetic transition at 2 K for fields below 70 kOe. The calculated effective moments per rare earth atom are close to the expected free ion values of R^{3+} except for Sm which displays anomalous behavior in the paramagnetic state. The non-magnetic members of this series (Y, Lu) are characterized by an unusually large electronic specific heat coefficient ($\sim 60 \text{ mJ/molK}^2$) and temperature-independent susceptibility term ($\chi_0 \sim 0.003 \text{ emu/mol}$), indicative of a relatively large density of states at the Fermi surface.

Key words: magnetically ordered materials, X-ray diffraction, magnetic measurements, heat capacity, electronic transport

PACS: 81.10.Dn, 71.20.Eh, 75.30.Gw, 75.30.Kz

Corresponding author

Email address: avila@ameslab.gov (M. A. Avila).

1 Introduction

The RT_2X_2 family of ternary intermetallic compounds ($R = Y, La-Lu$; $T = Mn-Cu, Ru, Rh$, etc and $X = Si, Ge$) have been intensively studied for several decades due to the wide range of physical behaviors displayed by its members (1). Most RT_2X_2 compounds form in the $ThCr_2Si_2$ structure, space group $I4/mmm$. This body-centered structure has a single R site in tetragonal point symmetry which can give rise to highly anisotropic local moments at low temperatures, influencing the magnetic behavior in a tractable way that allows many of these compounds to be used as model systems.

Some works on the RFe_2Ge_2 series of this family have successfully established their chemical behavior such as crystal structure, lattice parameters and chemical bonds (2; 3; 4) and melting temperatures (5; 6). But so far the ground state properties of the RFe_2Ge_2 series haven't been as intensively studied as others (e.g. RCu_2Si_2 or RNi_2Ge_2), in part due to the fact that, whereas in these compounds Fe is in its non-magnetic spin-paired $3d^6$ state (3), many of the Fe -based impurities are strongly magnetic and, even in small quantities, can prevent precise determination of the main compound's bulk physical properties. For example, an early report claiming the occurrence of partial spontaneous magnetization of the Fe sub-lattice in some arc-melted RFe_2Ge_2 ingots (7) was not confirmed in subsequent studies (nor in this present one) and was almost certainly due to the presence of ferro- or ferrimagnetic second phases in the samples.

The understanding of the anisotropic magnetic behavior and ordering temperatures in this series has also suffered from the lack of single crystals of sufficient size and quality to allow direct measurements of orientation-dependent properties. Although small single crystals picked out of annealed ingots have been used for x-ray refinements (4), larger crystals have been reported only for $LaFe_2Ge_2$ and $CeFe_2Ge_2$ (8; 9; 10) grown by the Czochralski method. The latter compound has received special attention (8; 9; 10; 11; 12; 13) for being a non-magnetic heavy fermion system with $\gamma = 210 \text{ mJ/molK}^2$.

In this work, we present a detailed characterization of the anisotropic ground state properties for 11 compounds of the RFe_2Ge_2 series ($R = Y, Pr, Nd, Sm, Gd-Tm, Lu$) grown as clean single crystal plates (with dimensions as large as $4 \times 4 \times 0.2 \text{ mm}^3$) by the flux growth method using Sn as the solvent (14; 15; 16), a method which also helps avoid the inclusion of magnetic second phases in the samples. After describing the experimental procedures used for crystal growth and characterization, results will be presented separately for each compound including a discussion of whether our experiments confirm, correct or contradict any established or claimed properties reported by previous works, such as ordering temperatures and effective moments. We will finish with a

discussion on the trends observed along the series such as the dependence of ordering temperatures and effective/saturated moments on the de Gennes factor ($g_J - 1)^2 J(J + 1)$.

2 Experimental Details

All single crystals of the RFe_2Ge_2 series studied here were grown out of Sn flux (14; 15; 16). The crystals grow quite easily and for a relatively wide range of growth parameters. A typical procedure involved adding to a 2 ml alumina crucible about 5 g of Sn (99.99% purity), and 3-10 at% of (at least 99.95% purity) R, Fe and Ge elements in or close to the ratio of 1:2:2 respectively. A small excess of Fe seemed to facilitate the growths, and in several cases a ratio of 1:2.4:2.0 was used, although it was not crucial nor did it change the actual measured properties of the crystals. The crucible with starting elements was sealed in a quartz ampoule under partial argon atmosphere, which was then placed in a box furnace. The elements were dissolved in Sn by holding the temperature at 1200 °C for 1-2 hours, then the crystals grew while the temperature was reduced over 3-6 days to a chosen temperature varying between 500 °C and 800 °C (depending on solute concentration), at which point the ampoule was quickly removed from the furnace and the molten Sn flux decanted.

The crystals form with a plate-like morphology as shown in Fig. 1, with the c-axis normal to the plane of the plate. They typically have very smooth and clean surfaces, and any remaining Sn flux droplets solidified on a surface (see upper left of Fig. 1) can be easily removed with a scalpel or polish. Most crystals have at least one very well defined facet along the [100] a-axis. The incomplete surface formation seen on the right part of the crystal in Fig. 1 gives an insight into the growth dynamics, with more rapid dendritic growth in the [110] directions.

DC magnetization measurements as a function of field (up to 55 kOe or 70 kOe) and temperature (1.8 to 350 K) were performed in Quantum Design SQUID magnetometers. Temperature sweeps were performed on warming, after zero-field cooling the sample to 1.8 K and applying a measuring field of 1 kOe. The samples were manually aligned to measure the magnetization along the appropriate axis. The notation $H_{||c}$ or $_c$ denotes measurements made with the applied field along the c-axis (field perpendicular to the plate shown in Fig. 1). $H_{\perp c}$ or $_{ab}$ denotes measurements made with the field in the basal plane (along the plate shown in Fig. 1), and $H_{||a}$ or $_a$ denotes measurements made with the field along a specific in-plane orientation: $H_{||[100]}$. Polycrystalline averages were calculated by $\langle T \rangle = [2 \langle T \rangle_{ab} + \langle T \rangle_c]/3$. These averages were used to obtain the high temperature effective moments of the magnetic rare



Fig. 1. A s-grown single crystal of TbFe_2Ge_2 on a millimeter-scale paper. The round droplet on the upper left is solidified Sn flux. Dendritic growth along the $[110]$ directions can be seen on the right side of the crystal.

earths, using a Curie-Weiss law : $\chi(T) = C/(T - T_p) + \chi_0$, including a temperature independent term to account for the relatively high susceptibility found in the non-magnetic members of the series. Values of χ_0 used are presented along with other measured properties in table 1. Neel temperatures were determined by the maximum in $d(\chi)/dT$, the temperature dependence of which near the transition of an antiferromagnet is similar to that of the magnetic specific heat(17). This derivation procedure enhances noise and two spurious features frequently appear in these data: one just above 4.2 K due to difficulties in the MPM S temperature control when the systems pass through the He boiling point, and another around 12 K most likely due to the fact that the MPM S systems change thermometers in this region.

Heat Capacity measurements were made on Quantum Design PPM S systems and in some cases a ^3He cooling option was installed, allowing measurements down to 0.4 K. Before each run the sample holder + grease background was measured for later subtraction from the sample + background data. Estimate

of the magnetic specific heat of samples with moment-carrying rare earths was made rather difficult due to the non-trivial behavior of the measured specific heats $C_p(T)$ even for $R = Y$ and Lu (shown in the following section). Similar difficulties have been reported for polycrystalline $PrFe_2Ge_2$ (18). To obtain our best estimate of the magnetic contribution $C_m^{(R)}(T) = C_p^{(R)}(T) - C_{nm}^{(R)}(T)$, where $C_p^{(R)}(T)$ is the measured specific heat and $C_{nm}^{(R)}(T)$ is the non-magnetic contribution for the rare-earth R , we fitted the specific heats of $LuFe_2Ge_2$ and YFe_2Ge_2 in the region $11\text{ K} < T < 45\text{ K}$ with a polynomial $T + AT^3 + BT^5 + CT^7$. The region below 11 K was avoided in the fits because of some low temperature features appearing in both samples which will be discussed later, but the resulting polynomials were then extended to represent $C_p^{(Lu)}(T)$ and $C_p^{(Y)}(T)$ in the full temperature range. We then used an interpolation formula $C_{nm}^{(R)}(T) = C_p^{(Lu)}(T) - (C_p^{(Lu)}(T) - C_p^{(Y)}(T))[(M_R^{3=2})/(M_{Lu}^{3=2} - M_Y^{3=2})]$, where M is the atomic mass of the respective rare earth indicated in the subscript, to remove the non-magnetic part $C_{nm}^{(R)}(T)$ of each compound's specific heat. This procedure gives a better estimate of the non-magnetic contribution than direct subtraction of $LuFe_2Ge_2$ and avoids the unphysical situation of $C_p^{(R)}(T) < C_{nm}^{(R)}(T)$ for a wider temperature range.

The magnetic entropy $S_m(T)$ of each sample was estimated by numerical integration of $C_m(T) = T \text{ vs: } T$. A simple linear extrapolation from the data measured at the lowest temperature down to the origin was used to represent $C_m(T)$ in the unmeasured region, in general the errors in $S_m(T)$ introduced by this simplification are smaller than those resulting from the subtraction of the non-magnetic contributions discussed above. To give an idea of the latter, in figure 4b we have included an estimation of $S_m(T)$ resulting after direct subtraction of $C_p(T)$ for $LuFe_2Ge_2$ to obtain $C_m(T)$ for $NdFe_2Ge_2$. At 20 K the difference adds up to only 4%. $S_m(T)$ is useful to give a basic idea of the degeneracy Z of the ground states involved in the magnetic ordering process, since at the transition $S_m(T)$ should approach $R \ln Z$, where $R = 8314\text{ J/mol K}$ is the universal gas constant. For some compounds the interference of nuclear Schottky anomalies at low temperatures as well as closely spaced, higher temperature (T & T_N) Schottky anomalies from low-lying CEF levels did not allow a reliable estimate of magnetic entropies.

Electrical resistance measurements were performed on Quantum Design PPM S systems or on Quantum Design MPM S systems operated in external device control (EDC) mode, in conjunction with Linear Research LR 400/LR 700 four-probe ac resistance bridges, allowing measurements down to 1.8 K. The electrical contacts were placed on the samples in standard 4-probe geometry, using Pt wires attached to a sample surface with either Epotex H 20e or Ablebond 88-1 silver epoxy, cured at 120 C for 30 minutes. The configuration was $I_{jj}[100]$; $H_{jj}[001]$ for samples with easy-axis magnetization, and $I_{jj}[100]$; $H_{jj}[010]$ for samples with easy-plane magnetization. Resistivity estimates for some sam-

ples were obtained from the resistance measurements by cutting the samples into rectangular slabs and estimating their cross-sections and voltage contact distances, but since many of these samples are quite thin the uncertainty in the absolute value of $\rho(T)$ is in the range of 20%. The resistive transition temperatures were estimated from jumps or peaks in $d\rho/dT$ which often behaves in a manner very similar to $C_m(T)$ and $d\rho(T)/dT$ near antiferromagnetic transitions (19; 20; 21).

Residual resistivity ratios are defined in this work as $RRR = \rho(300\text{ K})/\rho(1.8\text{ K})$, and in many cases the obtained value is a lower limit since there is still a finite slope in $\rho(T)$ at 1.8 K. When measured in zero applied field, $\rho(T)$ for most samples was found to drop 1% to 6% below 4 K due to the onset of superconductivity in very small droplets of Sn flux that remained on some of the sample surface. To estimate RRR correctly, this effect must be eliminated by applying a field above 0.3 kOe to drive Sn into its normal state. Given that the change in $\rho(T)$ is so small at the T_c of Sn, we can rule out the possibility of normal-state elemental Sn shorting out any significant percentage of the sample and giving rise to a spuriously high RRR. This is supported by the fact that there is no correlation between the percentile drops and the RRR values (see table 1). For example, even in the extreme case of a 20% drop for $R = Y$ (see inset fig. 2c) the sample RRR did not result among the highest values in the series. The percentile drops due to superconducting Sn are visible in the magnetoresistance graphs at 2 K for most samples, and in this case the data was normalized to $R(1\text{ kOe})$ instead of $R(0)$ to avoid this influence in the analysis as well.

3 Characterization of the compounds

3.1 YFe_2Ge_2 and $LuFe_2Ge_2$

Prior to this work, the only reported properties of YFe_2Ge_2 were its crystal structure and cell parameters (4). $LuFe_2Ge_2$ is a previously unreported compound. Our refinements of the x-ray diffraction pattern for YFe_2Ge_2 resulted in $a = 3.968(2)\text{ \AA}$, $c = 10.463(1)\text{ \AA}$, $V = 164.82(2)\text{ \AA}^3$. $LuFe_2Ge_2$ resulted in the same $I4mm$ space group as most other RT_2X_2 compounds, with $a = 3.914(1)\text{ \AA}$, $c = 10.395(1)\text{ \AA}$, $V = 159.27(2)\text{ \AA}^3$.

The magnetic behavior of both compounds is quite similar. Figure 2a shows the magnetic susceptibilities $\chi(T)$ at $H = 1\text{ kOe}$ which are, to a first approximation, Pauli-paramagnetic and slightly anisotropic with $\chi_{ab}(T) > \chi_c(T)$. This anisotropy is opposite to the case of non-magnetic RNi_2Ge_2 crystals (22), and the average molar susceptibility for the $T = Fe$ crystals ($\chi_0 = 0.003\text{ emu/mol}$)

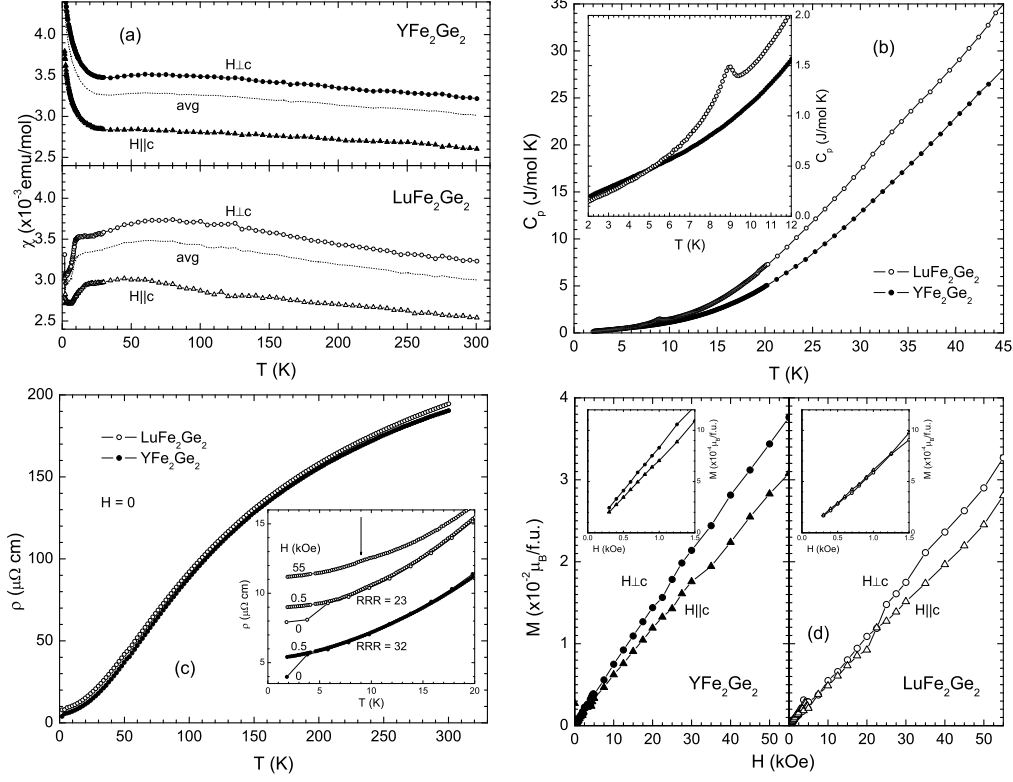


Fig. 2. Measurements on YFe_2Ge_2 and LuFe_2Ge_2 single crystals. (a) Anisotropic susceptibility at $H = 1$ kOe and polycrystalline averages. (b) Heat capacity at $H = 0$. The inset details the low temperature region. (c) Resistivity at $H = 0$. The inset shows low temperature resistivity for $H = 0$ and $H = 0.5$ kOe of both compounds, plus $H = 55$ kOe for LuFe_2Ge_2 . (d) Magnetization isotherms at $T = 2$ K. The insets detail the low-field region.

is also about an order of magnitude higher than for the TiNi ones. This is a notably large ρ_0 and, as will be discussed below, must be taken into account when analyzing the Curie tails of moment-bearing members of the series. At low temperatures, the YFe_2Ge_2 samples showed a small upturn probably due to a small amount of magnetic impurities (for example, the tail could be equivalent to that produced by a contamination of 0.1% Gd). In contrast, the low temperature behavior of LuFe_2Ge_2 showed a small but well marked anomaly at 9 K (we will discuss this feature after presenting the other measured properties in this compound where anomalies also appeared at this temperature).

Figure 2b shows the measured specific heats of both compounds. $C_p(T)$ increases monotonically between 2 K and 45 K for YFe_2Ge_2 , whereas a peak centered at 9 K occurs for LuFe_2Ge_2 (see inset), accompanying the reduction in susceptibility. When plotted as C_p/T vs: T^2 a linear region is observed between 11 K and 20 K, which extrapolates to 60 mJ/molK^2 for both compounds. This is a rather high value for the electronic specific heat coefficient, about 5 times larger than the values obtained for RNi_2Ge_2 , but comparable

to the value of 37 mJ/molK^2 estimated by Ebihara et al.(8) in single crystal LaFe_2Ge_2 , and consistent with the larger γ_0 terms found in the moment bearing compounds (see table 1). Below 11 K, $C_p^{(\text{Lu})}=T$ is obviously non-linear due to the transition at 9 K, and $C_p^{(\text{Y})}=T$ has a small upward deviation from linearity, of unknown origin. The estimated Debye temperatures from the slope of the same linear region mentioned above are $\theta_D = 280 \text{ K}$ and $\theta_D = 240 \text{ K}$ for $R = \text{Y}$ and Lu respectively.

The in-plane resistivity behaviors of YFe_2Ge_2 and LuFe_2Ge_2 are almost identical, as shown in figure 2c. Starting at $\rho_{xx} = 200 \text{ cm}$ at room temperature, they decrease monotonically with a broad curvature upon cooling, followed by an inflexion point around 70 K, and finally tends to saturate at the lowest temperatures. The inset shows the low temperature behavior for $H = 0.5 \text{ kOe}$, where $\rho_{xx}(T)$ reaches 5.4 and 9.0 cm at 1.8 K, resulting in RRR values of 32 and 23 for $R = \text{Y}$ and Lu respectively, in good agreement with those obtained for $R = \text{La}$ and Ce single crystals(8) and annealed ingots(13). These values are almost 10 times larger when compared to the $T = \text{Ni}$ crystals, and can be understood as a combined effect of a residual resistivity $\rho(0)$ 3-4 times smaller, with resistivity at room temperature 2-3 times larger. The former feature demonstrates the high crystallographic quality of the $T = \text{Fe}$ crystals, and the latter points to a characteristic effect of the $T = \text{Fe}$ compounds above 70 K, which increases electron scattering and results in the broad curvature up to 300 K. The inset of fig. 2c also shows $\rho_{xx}(T)$ at 55 kOe for LuFe_2Ge_2 , where a very subtle anomaly around 9 K is observed.

The field-dependent magnetizations of YFe_2Ge_2 and LuFe_2Ge_2 at 2 K are weakly anisotropic and essentially linear below $H = 55 \text{ kOe}$ (fig. 2d). The insets show how linearity is maintained down to 0.3 kOe and essentially extrapolate to the origin (at 2 K the Sn droplets become superconducting just below 0.3 kOe, leading to small diamagnetic net response). This behavior demonstrates the absence of secondary ferromagnetic phases in these samples.

The 9 K transition observed in LuFe_2Ge_2 appears to be a robust feature which is very likely an intrinsic property of this compound. It was observed as a loss of about 10% in the susceptibility of two different samples from different growth batches, and was little affected by applied fields up to 55 kOe. It is accompanied by a peak in heat capacity which amounts to $C_p = C_p(T_0) + 20\%$, with transition width $T_0 = T_0 \pm 9\%$, and a subtle feature in the in-plane resistivity. One possible explanation is the formation of a spin- or charge-density wave which would abruptly decrease the susceptibility by opening a gap in part of the Fermi surface. Using the γ_0 value obtained above, we estimate $C_p = T_0 \pm 0.46$, about 30% of the BCS value of 1.43 expected in the mean field approximation(23), which would imply a significant nesting effect on the Fermi surface. If so, the nesting would most likely be along the [001] direction given the small change in $\rho_{xx}(T)$ around 9 K for $I \parallel [001]$. But

obviously these are only rough estimates and further investigation, including out-of-plane resistivity measurements, will be required to confirm or refute this hypothesis.

3.2 PrFe_2Ge_2

Earlier investigations(18; 24; 25; 26; 27; 28) in PrFe_2Ge_2 ingots and powders have reported that this compound is an antiferromagnet with $T_N = 14$ K, and a second transition temperature at 9 K which separates two different ordering regimes: a low-temperature AF II-type magnetic structure consisting of ferromagnetic layers of Pr moments aligned along the c-axis in a ++ pattern, and a higher temperature incommensurate magnetic structure where the moments remain aligned with the c-axis but with an amplitude modulated sinusoidally along the same axis. The ordered magnetic moment was found close to the expected value of $3.2 \mu_B$ for Pr^{3+} . Field-dependent magnetization measurements in the ordered state also showed a single metamagnetic transition near 15 kOe.

The susceptibility at $H = 1$ kOe of single crystal PrFe_2Ge_2 is strongly anisotropic (figure 3a). For $H \parallel c$ the susceptibility increases strongly as the sample is warmed, presenting two transitions marked by a sharp jump at the lower one and a well defined peak at the higher one, after which $\chi_c(T)$ decreases monotonically up to 300 K. For $H \perp c$ the susceptibility is much smaller and decreases monotonically from 1.8 K, with a larger slope between the two aforementioned transition temperatures. Analysis of the peaks in $d(\chi)/dT$ (fig. 3b) places the two transition temperatures at 8.3 K and 14.6 K respectively (as discussed in the experimental methods section, the features near $T = 4.2$ and 12 K are spurious, can be seen in many of the $d(\chi)/dT$ data sets, and will not be discussed further). Fitting the polycrystalline average $\chi(T)$ above 20 K yields $\chi_{\text{eff}} = 3.5 \mu_B/\text{f.u.}$, close to the free ion value of $3.57 \mu_B/\text{f.u.}$ for Pr^{3+} .

Specific heat measurements (fig. 3b) show a very sharp rise as the sample is cooled below 15 K, which peaks at 14.6 K marking the transition between disordered and ordered magnetic states, and then a broad curvature with only a subtle change in slope at 8.2 K (which nonetheless appears as a peak in the derivative of this curve) that marks the transition between different magnetically ordered phases. Below 3.2 K the specific heat begins to rise strongly again, probably due to a nuclear Schottky effect. Neglecting this rise, the estimated magnetic entropy reaches 4.3 J/mol K , somewhat short of $R \ln 2 = 5.75 \text{ J/mol K}$, most likely due to an overestimate of the lattice contribution when obtaining $C_m(T)$.

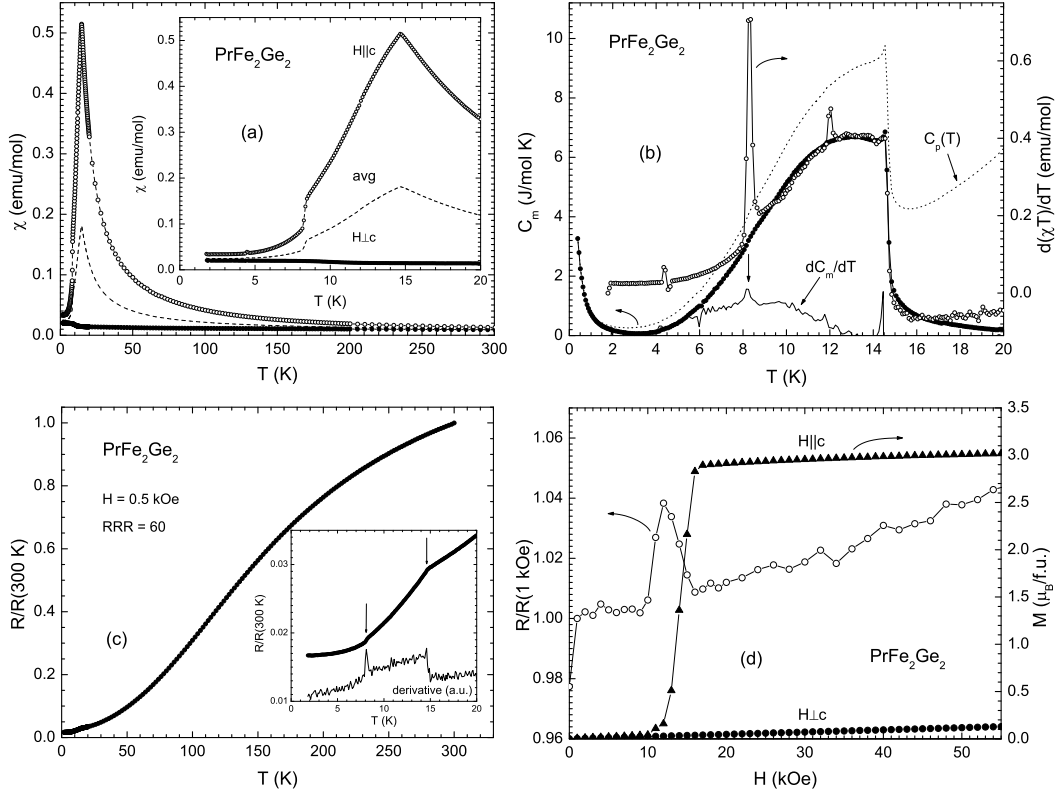


Fig. 3. Measurements on PrFe_2Ge_2 single crystals. (a) Anisotropic susceptibility at $H = 1$ kOe and polycrystalline average. (b) Magnetic heat capacity at $H = 0$ (solid symbols), its derivative (solid line) and $d(\chi T)/dT$ from the susceptibility average (open symbols). The dotted line shows the raw heat capacity data. (c) Normalized resistance at $H = 0.5$ kOe. The inset details the low temperature region (left scale) and $d(\chi T)/dT$ (arbitrary units). (d) Magnetization isotherms at $T = 2$ K (solid symbols) and normalized magnetoresistance (open symbols).

Normalized resistance measurements at $H = 0.5$ kOe (Fig. 3c) show the same general behavior as those of the non-magnetic compounds, but with $\text{RRR} = 60$ and two well marked changes in slope at 8.2 K and 14.6 K, as a consequence of changes in the spin-disorder scattering regimes for different magnetic phases.

Field-dependent magnetization at $T = 2$ K shows an almost perfectly linear behavior for $H \parallel c$, reaching a value of $0.13 \mu_B/\text{f.u.}$ at 55 kOe. For $H \parallel ab$ the behavior is initially similar, with a slope about 1.8 times larger, followed by a jump of $2.9 \mu_B/\text{f.u.}$ between 10 and 16 kOe consistent with a spin-op transition of the Pr moments, then adopts a similar slope as for $H \parallel c$, reaching a value of $3.0 \mu_B/\text{f.u.}$ at 55 kOe. We found no evidence of a transition at 1 kOe claimed in a previous work on polycrystals (29), which was more likely an extrinsic effect due to small ferromagnetic impurities. Normalized magnetoresistance at 2 K is small and positive, showing a sharp peak during the spin-op transition, and finally resumes a featureless positive slope reaching about 8% increase at 90 kOe.

3.3 NdFe₂Ge₂

Earlier works on NdFe₂Ge₂ ingots and powders(7; 26) have shown that its magnetic behavior is similar to PrFe₂Ge₂. It was claimed to order antiferromagnetically with $T_N = 13$ K, and to present the same AF II-type magnetic structure with moments along the c-axis.

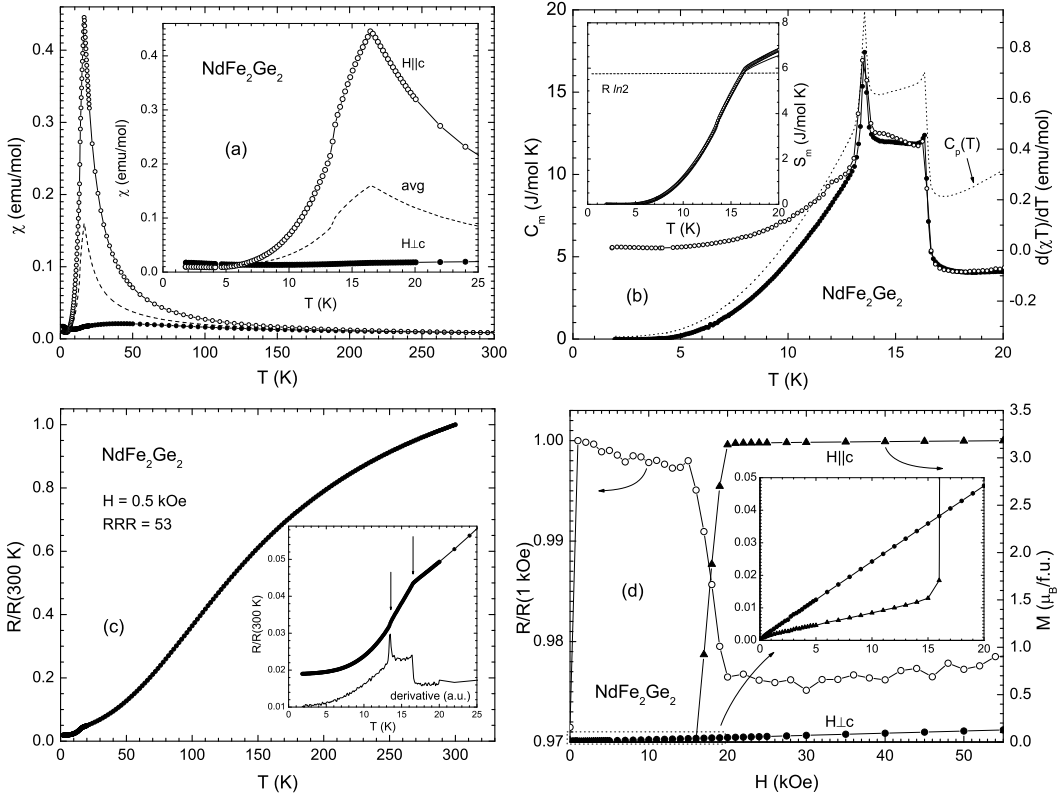


Fig. 4. Measurements on NdFe₂Ge₂ single crystals. (a) Anisotropic susceptibility at $H = 1$ kOe and polycrystalline average. (b) Magnetic heat capacity at $H = 0$ (solid symbols) and $d\chi/dT$ from the susceptibility average (open symbols). The dotted line shows the raw heat capacity data. The inset shows the magnetic entropy as calculated from our standard procedure (open circles), and the solid line is the result obtained after direct subtraction of the LuFe₂Ge₂ specific heat. (c) Normalized resistance at $H = 0.5$ kOe. The inset details the low temperature region (left scale) and $d\chi/dT$ (arbitrary units). (d) Magnetization isotherms at $T = 2$ K (solid symbols) and normalized magnetoresistance (open symbols). The inset details the low field region.

The temperature dependent susceptibility of single crystal NdFe₂Ge₂ is strongly anisotropic (e.g. 4a) and indeed similar to PrFe₂Ge₂ in general terms. $\chi_c(T)$ initially decreases slightly as temperature is raised from 1.8 K, then rises fast and shows two transitions marked by a jump and a sharp peak, after which it decreases in a roughly Curie-Weiss like manner. $\chi_{ab}(T)$ is initially larger than $\chi_c(T)$ at the lowest temperatures, decreasing below $\chi_c(T)$ as the temperature

is raised, and then exhibits a very broad peak centered at around 40 K, indicating a CEF level splitting within this thermal energy range. Analysis of the peaks in $d(T)/dT$ (g. 4b) places the two transition temperatures at 13.5 K and 16.4 K respectively, so the previously reported transition observed in ingots may actually have been the lower one. Fitting $C_m(T)$ above 20 K yields $C_{eff} = 3.4 \text{ }_B/\text{f.u.}$, close to the free ion value of $3.61 \text{ }_B/\text{f.u.}$ for Nd^{3+} .

The magnetic specific heat of NdFe_2Ge_2 shows a sharp rise which peaks at 16.4 K and, unlike PrFe_2Ge_2 , the lower transition is also marked by a sharp peak at 13.5 K (g. 4b). After this lower peak C_m drops monotonically down to the lowest measured temperature of 2 K, with no indication of any further features. The total magnetic entropy accumulated up to the 16.4 K transition is approximately $R \ln 2$, and continues to rise slowly above this temperature, consistent with the presence of other CEF levels contributing in this region (as discussed in the experimental methods section, we used two different methods to account for the non-magnetic component of the specific heat for these data. There is virtually no difference for $T < T_N$ in this case).

The high temperature behavior of the normalized resistance at $H = 0.5 \text{ kOe}$ (g. 4c) is similar to PrFe_2Ge_2 , and the low temperature region (inset) shows two well marked changes in slope at 16.4 K and 13.5 K, followed by a lower temperature levelling-off which results in $RRR = 53$. The derivative dR/dT makes the two transitions even clearer and shows a temperature dependence that is very similar to that seen for $C_m(T)$ and $d(T)/dT$.

The field-dependent magnetization at 2 K is shown in (g. 4d). The planar magnetization is almost perfectly linear with field and has a small slope, reaching $0.11 \text{ }_B/\text{f.u.}$ at 55 kOe. The axial magnetization begins rising with a smaller slope than the planar one, but then undergoes a jump of $3.1 \text{ }_B/\text{f.u.}$ between 15.5 and 20 kOe, then essentially saturates, reaching $3.2 \text{ }_B/\text{f.u.}$ at 55 kOe. In a similar manner, the normalized magneto-resistance starts with a small negative slope as the field is increased, followed by a sharp 2% drop between 15 and 20 kOe accompanying the spin-op transition seen in magnetization, and finally a small positive slope which persists up to 90 kOe consistent with saturation of the Nd moments.

3.4 SmFe_2Ge_2

SmFe_2Ge_2 has been very little explored until now. Only the crystal structure and lattice parameters were determined (3), ^{57}Fe Mossbauer spectroscopy was performed at 77 K and 300 K (3), and its melting temperature was measured (5; 6). To the best of our knowledge, no characterization of its low-temperature properties has been previously reported.

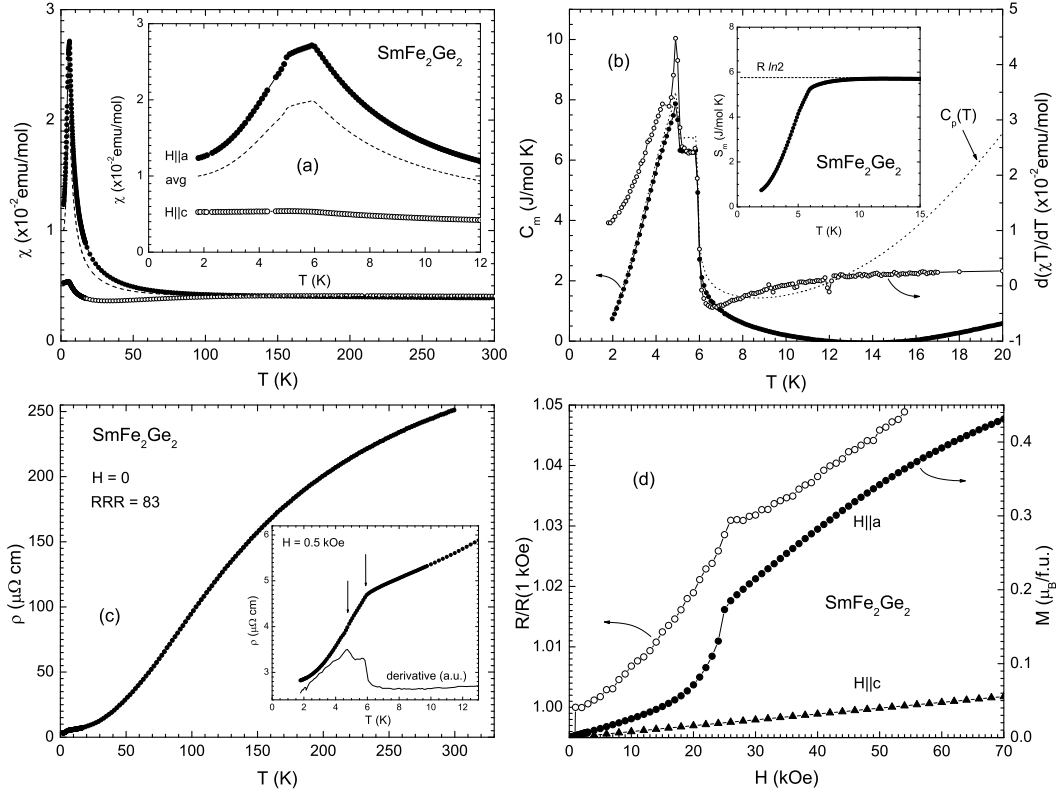


Fig. 5. Measurements on SmFe_2Ge_2 single crystals. (a) Anisotropic susceptibility at $H = 1$ kOe and polycrystalline average. (b) Magnetic heat capacity at $H = 0$ (solid symbols) and $d(\chi T)/dT$ from the susceptibility average (open symbols). The dotted line shows the raw heat capacity data. The inset shows the magnetic entropy. (c) Resistivity at $H = 0.5$ kOe. The inset details the low temperature region (left scale) and $d(\chi T)/dT$ (arbitrary units). (d) Magnetization isotherms at $T = 2$ K (solid symbols) and normalized magnetoresistance (open symbols).

Our susceptibility measurements (Fig. 5a) showed anisotropic behavior at temperatures up to about 120 K, with $\chi_a(T)$ being significantly larger than $\chi_c(T)$ in this region. $\chi_a(T)$ increases rapidly with increasing temperature, and shows a well-marked double transition somewhat similar to those observed in the Pr and Nd compounds, very likely indicating antiferromagnetic ordering with moments aligned in or close to the ab -plane and two distinct magnetic structures. Above the higher transition temperature $\chi_a(T)$ drops, but in a distinctly non-Curie-Weiss manner. $\chi_c(T)$ initially rises until the lower transition temperature is reached, then drops into a broad minimum centered at 33 K, and finally rises again until towards $\chi_a(T)$. The transition temperatures determined from the peaks in $d(\chi T)/dT$ are 4.9 K and 5.9 K (Fig. 5b). Both curves assume essentially the same levelled value of 0.004 emu/mol above 120 K, very similar to that of the $R=Y$ and Lu compounds, indicating that the Sm ions essentially become non-magnetic either due to thermal population of the upper Hund's rule multiplet or shift in the valency from $3+$ towards $2+$ with increasing temperature. Similar magnetic behavior was pre-

viously observed in SmNi_2Ge_2 single crystals(22). Fitting $\chi(T)$ above 20 K yields $\chi_{\text{eff}} = 0.46 \mu_B/\text{f.u.}$, significantly smaller than the free ion value of $0.84 \mu_B/\text{f.u.}$ for Sm^{3+} .

The magnetic specific heat (Fig. 5b) rises sharply on cooling through the upper transition temperature of 5.9 K, then displays a plateau followed by a peak at 4.9 K and roughly linear drop down to 2 K. The accumulated magnetic entropy at 5.9 K is very close to $R \ln 2$ and then essentially levelled up to 20 K, indicating a ground state doublet well separated in energy from other excited levels.

The zero-field resistivity of SmFe_2Ge_2 (Fig. 5c) starts at 250 $\mu\Omega\text{cm}$ and drops as the previously reported members until a sharp change in slope marks the decrease of spin-disorder scattering at 5.9 K. The lower transition at 4.9 K isn't readily seen, but appears as a peak centered at 4.8 K in the derivative plot. For this sample $\text{RRR} = 83$ is one of the highest values obtained in the series.

Field-dependant magnetization at $T = 2 \text{ K}$ (Fig. 5d) shows a broad metamagnetic transition ending at 25 kOe for $H \parallel a$, and then continues to rise, reaching $0.43 \mu_B/\text{f.u.}$ at the highest measured field of 70 kOe. The finite slope at this field indicates that the magnetization is not yet saturated. Magnetization for $H \parallel c$ is linear with field and reaches $0.055 \mu_B/\text{f.u.}$ at 70 kOe. Magnetoresistance is positive and shows a feature around 25 kOe, marking the metamagnetic transition.

3.5 GdFe_2Ge_2

GdFe_2Ge_2 is one of the members that has been receiving special attention in recent years both by itself(30) and as part of the GdT_2Ge_2 group (31; 32), taking advantage of the fact that the spherically symmetric, half-filled 4f shell of Gd^{3+} reduces the influence of hidden anisotropies in polycrystals, simplifying the application of molecular and crystal field models and derivation of relevant parameters. The most recent work by Duong et al.(30) presents a detailed study on single-phase annealed ingots and powders. Besides confirming the antiferromagnetic ordering at 11 K reported in earlier works(7; 24; 33), their main results are a deviation from Curie-Weiss behavior in $\chi^{-1}(T)$, a saturated magnetization in $M(H)$ at 4.2 K that falls somewhat shy of the expected value of $7 \mu_B/\text{f.u.}$, and a magnetic specific heat behavior $C_m(T)$ that peaks at 9.6 K on cooling, followed by a broad anomaly around 3 K. All these features were explained based on a generalized molecular-field model where the Gd moments interact with an itinerant-electron band.

As expected, the temperature dependent susceptibility at $H = 1 \text{ kOe}$ of single

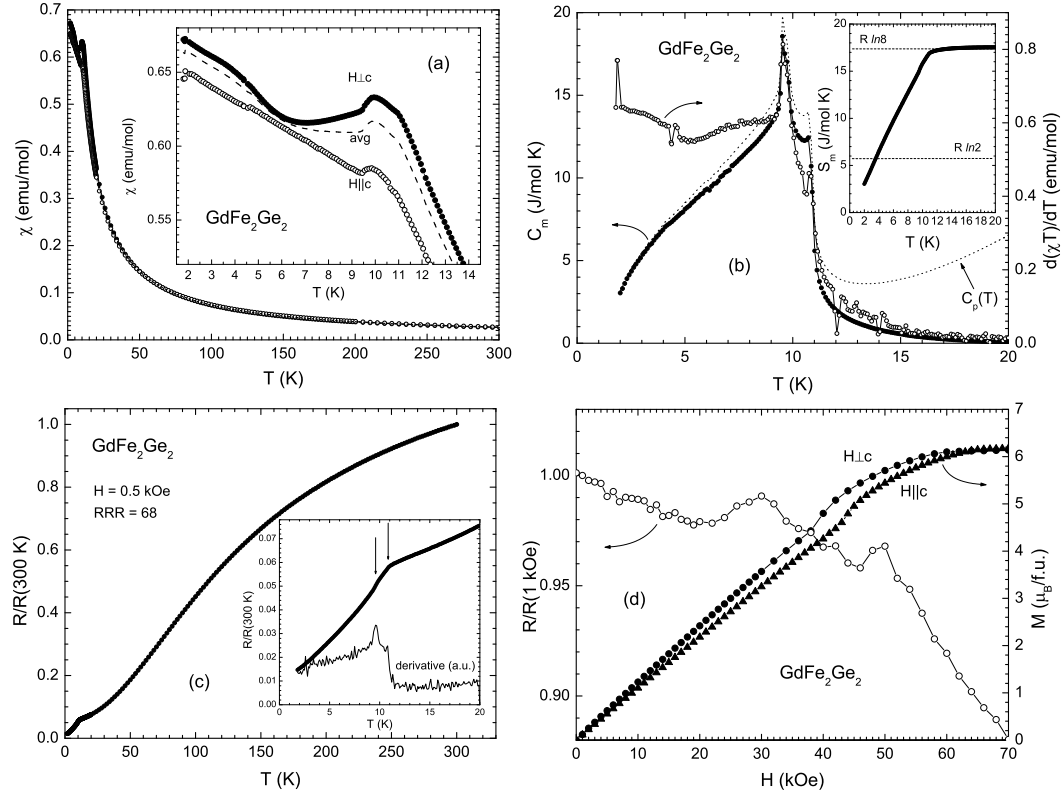


Fig. 6. Measurements on GdFe_2Ge_2 single crystals. (a) Anisotropic susceptibility at $H = 1$ kOe and polycrystalline average. (b) Magnetic heat capacity at $H = 0$ (solid symbols) and $d(\chi T)/dT$ from the susceptibility average (open symbols). The dotted line shows the raw heat capacity data. The inset shows the magnetic entropy. (c) Normalized resistance at $H = 0.5$ kOe. The inset details the low temperature region (left scale) and $d(\chi T)/dT$ (arbitrary units). (d) Magnetization isotherms at $T = 2$ K (solid symbols) and normalized magnetoresistance (open symbols).

crystal GdFe_2Ge_2 in the paramagnetic state is essentially isotropic (Fig. 6a), with $\chi_{ab}(T)$ slightly higher than $\chi_c(T)$ (consistent with the non-magnetic members of the series). The low temperature behavior is quite rich, with the susceptibility undergoing several changes in slope up to 11 K, after which it drops monotonically. By taking $\chi_0 = 0.0026$ emu/mol into account there is no significant deviation from Curie-Weiss behavior above 20 K, and the fit of $\chi(T)$ yields $\chi_{\text{eff}} = 7.6 \mu_B/\text{f.u.}$, a little lower than the expected value of $7.94 \mu_B/\text{f.u.}$ for free-ion Gd^{3+} . Analysis of $d(\chi T)/dT$ (Fig. 6b) shows a large sharp peak at 9.6 K and a smaller sharp peak/break at 10.8 K.

The magnetic specific heat of GdFe_2Ge_2 is also rich in features (Fig. 6b). It shows a sharp rise with a small peak centered at 10.8 K on cooling, then continues rising towards a larger peak at 9.6 K and finally displays a broad shoulder around 3.0 K which has been observed in some other Gd compounds such as GdB iPt (34) and GdCu_2Si_2 (35) and in the latter case it was attributed by the authors to a small Zeeman splitting of the ground state octuplet in

the ordered state. The magnetic entropy reaches $R \ln 8$ at the higher transition temperature, as expected for a Gd ground state octuplet. These features and values are all in excellent agreement with ingots measured by Duong et al., except that for our crystals we were able to resolve two very distinct transitions.

Normalized resistance as a function of temperature (g. 6c) clearly shows a loss of spin-disorder scattering below 10.9 K, and a second, subtle change in slope at 9.6 K (easily seen as a peak in the derivative) marking the lower transition. Again, there is a clear similarity between $d\rho/dT$ and $C_m(T)$ and $d(T)\rho/dT$. For this sample $R/R_R = 68$.

The field-dependent magnetization at 2 K starts increasing linearly, with the planar orientation slope slightly larger than the axial one (g. 6d). A clear change in behavior occurs at 38 kOe and 43 kOe respectively, where magnetization seems to show a small metamagnetic jump and then curves towards saturation, reaching a value of $6.2 \mu_B/\text{f.u.}$ at 70 kOe. This value is essentially the same as that reported for powders at 70 kOe, but high field measurements on these show that the magnetization continues to increase slowly until just below $7 \mu_B/\text{f.u.}$ at 400 kOe (30). Normalized magneto-resistance starts with a small negative slope, then shows some rather ill-defined features between 30 kOe and 50 kOe, and finally increases its slope reaching a 12% drop at 70 kOe.

3.6 TbFe₂G_e₂

TbFe₂G_e₂ was first reported as having antiferromagnetic ordering below 7.5 K and a metamagnetic transition at 15 kOe in $M(H)$ measured at 4.2 K (24). Neutron diffraction experiments later described it as showing axial antiferromagnetic ordering below 7.5 K with an incommensurate magnetic structure (36), although another neutron diffraction work claimed that it was still paramagnetic at 4.2 K (37), and finally a more recent study that combined neutron diffraction with magnetization measurements showed antiferromagnetic ordering with $T_N = 8.5 \text{ K}$, $(1.5 \text{ K}) = 7.68 \mu_B/\text{Tb}$, an incommensurately modulated magnetic structure with two wave vectors, and a metamagnetic transition at $H = 11 \text{ kOe}$ for $T = 4.2 \text{ K}$ (38).

Strong anisotropies in the susceptibility exist for single crystal TbFe₂G_e₂ (g. 7a). The low temperature behavior of $\chi_c(T)$ for $H = 1 \text{ kOe}$ is dominated by a maximum at 8.2 K, with a corresponding maximum in $d(T)\rho/dT$ at $T_N = 7.4 \text{ K}$ (g. 7b). This may explain the 1 K discrepancy of ordering temperatures reported in literature, since apparently the authors reporting $T_N = 8.5 \text{ K}$ used the maximum in $\chi(T)$ as criterion. The susceptibility for

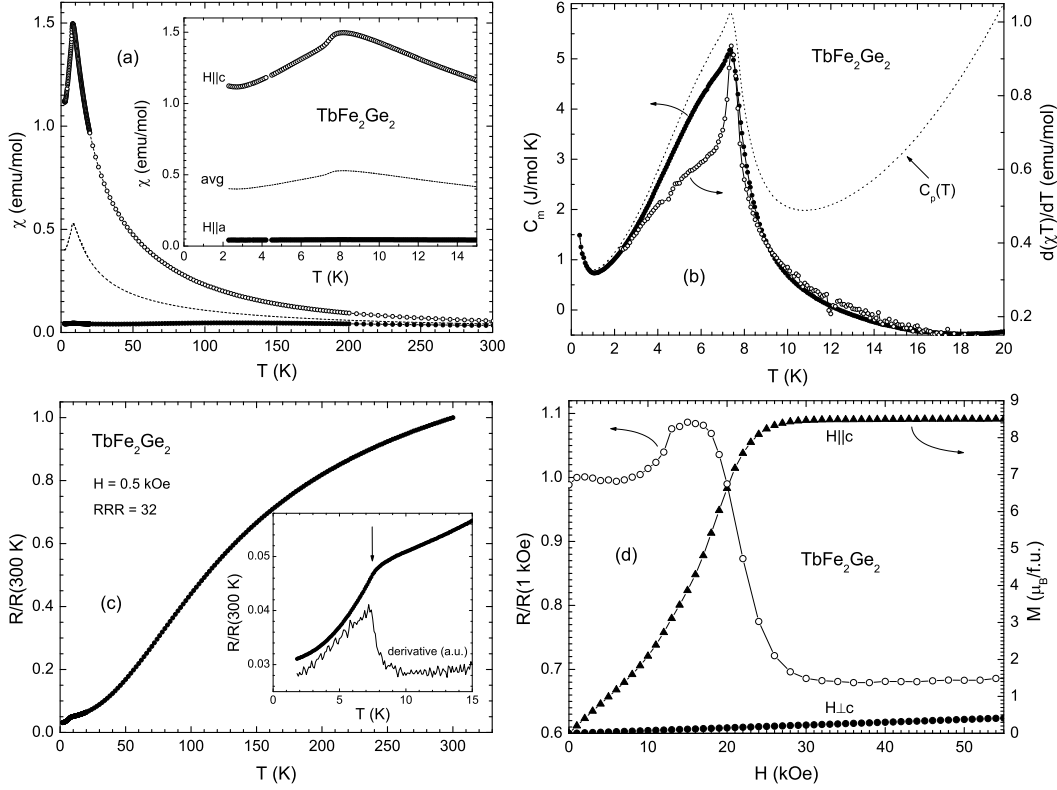


Fig. 7. Measurements on TbFe_2Ge_2 single crystals. (a) Anisotropic susceptibility at $H = 1 \text{ kOe}$ and polycrystalline average. (b) Magnetic heat capacity at $H = 0$ (solid symbols) and $d(\chi T)/dT$ from the susceptibility average (open symbols). The dotted line shows the raw heat capacity data. (c) Normalized resistance at $H = 0.5 \text{ kOe}$. The inset details the low temperature region (left scale) and $d(T)/dT$ (arbitrary units). (d) Magnetization isotherms at $T = 2 \text{ K}$ (solid symbols) and normalized magnetoresistance (open symbols).

$H_{\parallel a}$ is about 30 times smaller, but presents the same peak at 8.2 K and upturn at the lowest temperatures, which may indicate a small misalignment in the orientation or that the ordered Tb moments form a small angle with the c-axis. It also shows a very broad maximum centered at 120 K probably resulting from a CEF level split of comparable thermal energy. Fitting $C_p(T)$ above 20 K yields $\chi_{\text{eff}} = 9.6 \mu_B/\text{f.u.}$, close to the expected value of $\chi_{\text{eff}} = 9.72 \mu_B/\text{f.u.}$ for Tb^{3+} .

The magnetic specific heat (Fig. 7b) shows a more broadened rise near the transition as those observed in other members of the family. $C_m(T)$ reaches maximum value at 7.4 K, then decreases with a broad curvature down to 1 K, after which it starts rising again probably due to a nuclear Schottky effect. This feature makes the estimation of the magnetic entropy difficult. If the low temperature rise is ignored, the total entropy up to T_N reaches about 5 J/mol K, close to $R \ln 2$ given the qualitative nature of the low temperature extrapolation of our $C_p(T)$ data. For this sample the procedure for estimat-

tion of $C_m(T)$ did not work as well as with the others, since even with the corrections $C_m(T)$ becomes spuriously negative above 13 K.

Normalized resistance at $H = 0.5$ kOe (g. 7c) has essentially the same temperature dependence as the other members of the family, and presents a single, rather broad change in behavior near the ordering temperature due to loss of spin disorder scattering. For this sample $RRR = 32$, so the broadened features discussed here are probably not resulting from poorer sample quality.

The magnetization as a function of applied field at $T = 2$ K is strongly anisotropic (g. 7d). For $H \parallel c$ a broad upward curvature exists between 6 kOe and 20 kOe, indicative of a metamagnetic transition in this region. Above 30 kOe the magnetization essentially saturates, reaching $8.5 \mu_B/\text{f.u.}$ at 70 kOe, lower than the value of $9 \mu_B/\text{f.u.}$ for Tb^{3+} saturated moments. Application of the field parallel to the a -axis yields linear behavior, reaching $0.55 \mu_B/\text{f.u.}$ at 70 kOe. The magnetoresistance behavior starts practically flat, then rises 9% between 6 and 15 kOe, followed by a drop of almost 40% between 15 and 30 kOe, after which it adopts a very small positive slope up to 70 kOe.

All of the broadened features seen in different measurements of the transition in TbFe_2Ge_2 indicate that for this compound the behavior in this region could be a more washed-out version of the double transitions seen in previous compounds, with the higher magnetic phase existing in a very narrow temperature interval. On the other hand TbFe_2Ge_2 may simply have a single magnetic phase transition in low fields.

3.7 DyFe_2Ge_2

Few studies have been previously conducted on DyFe_2Ge_2 . Its crystal structure and lattice parameters were determined (2; 3) and more recently Szytula et al. characterized its magnetic behavior (38). The main reported results are: axial antiferromagnetic ordering below 3.35 K, ordered magnetic moment of $7.68 \mu_B/\text{f.u.}$ at 1.5 K, and an incommensurately modulated magnetic structure described by two wave vectors.

The magnetic susceptibility of single crystal DyFe_2Ge_2 (g. 8a) is less anisotropic than TbFe_2Ge_2 . The axial susceptibility has a maximum at 2.5 K, after which it drops rapidly. The planar susceptibility is similar, but with a magnitude about 10 times smaller and ill-defined behavior below 2.5 K. Fitting $\chi(T)$ above 20 K yields $\chi_{\text{eff}} = 10.6 \mu_B/\text{f.u.}$, essentially the expected value for Dy^{3+} . The peak in $d(\chi)/dT$ gives $T_N = 2.1$ K (g. 8b) although there could be some uncertainty in this value since we have only a few data points below 2.5 K. On the other hand, specific heat and resistivity data (discussed below) confirm this value.

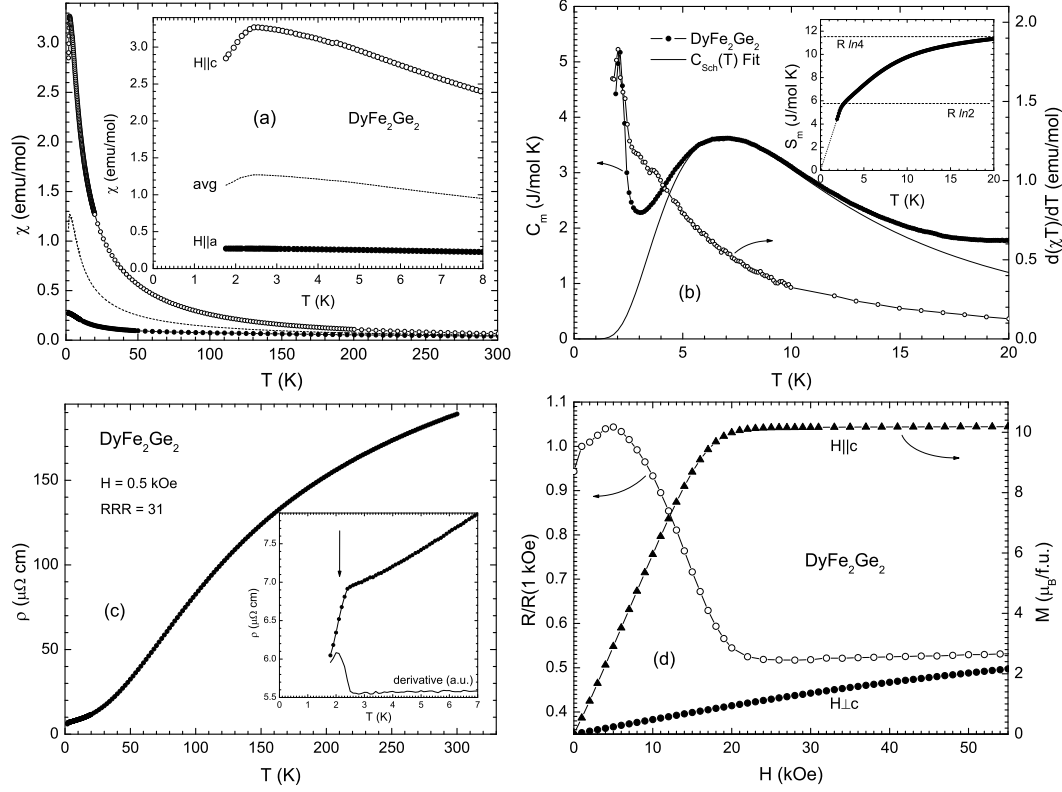


Fig. 8. Measurements on DyFe_2Ge_2 single crystals. (a) Anisotropic susceptibility at $H = 1 \text{ kOe}$ and polycrystalline average. (b) Magnetic heat capacity at $H = 0$ (solid symbols), $d(\chi T)/dT$ from the susceptibility average (open symbols) and that of eq. 1 (solid line). The inset shows the magnetic entropy, where the dotted line results from integration of the extrapolated $C_m(T)$ data to zero. (c) Resistivity at $H = 0.5 \text{ kOe}$. The inset details the low temperature region (left scale) and $d(T)=dT$ (arbitrary units). (d) Magnetization isotherms at $T = 2 \text{ K}$ (solid symbols) and normalized magnetoresistance (open symbols).

For clarity, the as-measured specific heat $C_p(T)$ for DyFe_2Ge_2 and also for $R = \text{Ho-Tm}$ will be shown separately in figure 9a. The magnetic specific heat $C_m(T)$ of DyFe_2Ge_2 (Fig. 8b) is characterized by a broad Schottky-like anomaly with local maximum at 6.8 K , below which a sharp peak at 2.1 K marks the magnetic ordering and confirms the value obtained from $d(\chi T)/dT$. The dashed curve in Fig. 8b is attributed to the Schottky contribution to magnetic specific heat for a two-level system given by

$$C_{\text{Sch}} = R \left(\frac{T}{\Delta} \right)^2 \frac{g_0}{g_1} \frac{e^{-\Delta/T}}{[1 + (g_0/g_1)e^{-\Delta/T}]^2}; \quad (1)$$

where $R = 8314 \text{ mJ/mol K}$ is the universal gas constant, Δ is the energy gap in K, and g_0/g_1 gives the ratio between the degeneracies of the lower and upper energy levels respectively. From this we obtain $\Delta = 16.5 \text{ K}$ and $g_0/g_1 = 1:0$.

The estimated magnetic entropy (inset) suffers from the lack of data points below 1.9 K, but is close to $R \ln 2$ at T_N and then approaches $R \ln 4$ at 20 K. Given that Dy is a Kramers ion, these data indicate that a pair of doublet ground states dominate the low temperature properties of this compound.

Resistivity for $H = 0.5 \text{ kOe}$ (g.8c) starts at $190 \text{ } \mu\Omega\text{cm}$ at room temperature, and decreases like all other members upon cooling until an abrupt change in slope occurs around 2.1 K, marking a significant reduction of spin-disorder scattering. At 1.8 K the resistivity is just above $6 \text{ } \mu\Omega\text{cm}$ and the resulting RRR for this sample is 31, although the sharp slope seen at this temperature indicates that this value is to be considered as a lower limit.

The field-dependent magnetization of DyFe_2Ge_2 at 2 K for $H \parallel c$ results in a rapidly increasing magnetization up to 22 kOe, above which it essentially saturates reaching $10.2 \text{ } \mu_B/\text{f.u.}$ at 55 kOe (g.8d). Applying the field in the basal plane results in slightly sublinear behavior, reaching $2.2 \text{ } \mu_B/\text{f.u.}$ at 55 kOe. Normalized magnetoresistance initially rises about 4% up to 5 kOe, then drops almost 50% until the Dy moments saturate at 22 kOe, and finally assumes a small positive slope with no further features up to 90 kOe. These data are all consistent with a metamagnetic transition that is complete for $H \parallel c$ 22 kOe.

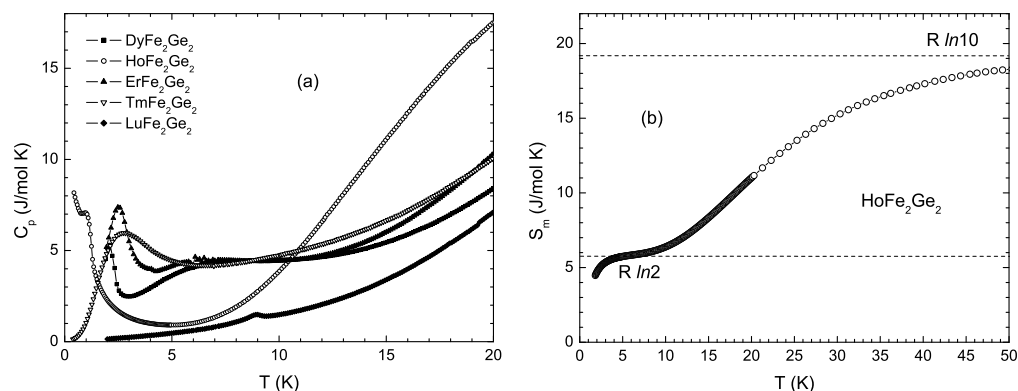


Fig. 9. (a) As measured heat capacities of RFe_2Ge_2 single crystals for $\text{R} = \text{Dy-Tm}$ and Lu . (b) Estimation of the magnetic entropy of HoFe_2Ge_2 , assuming $S_m(5 \text{ K}) = R \ln 2$.

3.8 HoFe_2Ge_2

An initial characterization of the magnetic properties of HoFe_2Ge_2 was reported in 1997 by Szytula et al. in the same work that characterized the compounds with $\text{R} = \text{Tb, Dy}$ (38). They found no sign of ordering down to 1.5 K, but neutron diffraction measurements indicated signs of long-range magnetic interactions that could lead to antiferromagnetic ordering at some lower temperature. In contrast, another work by Schobinger-Papamantellos et al. reported

that their HoFe_2Ge_2 samples showed axial arrangement of the moments below 17 K, with wave vector $(0.5, 0.5, 0)$. Short range order effects were reported below 6 K, and the moment at 1.5 K was estimated as $6.6 \mu_B$. Szytula et al. have recently performed new neutron diffraction experiments and found the same collinear antiferromagnetic structure which however disappears above 7 K, a short-range magnetic order which disappears above 5 K, and moment of $4.5 \mu_B$. The conclusion of the authors who performed these three studies was that HoFe_2Ge_2 represents a rare case of coexisting long-range and short-range orders, resulting from a competition between RKKY interactions and CEF effects, and leading to a frustration of the magnetic order.

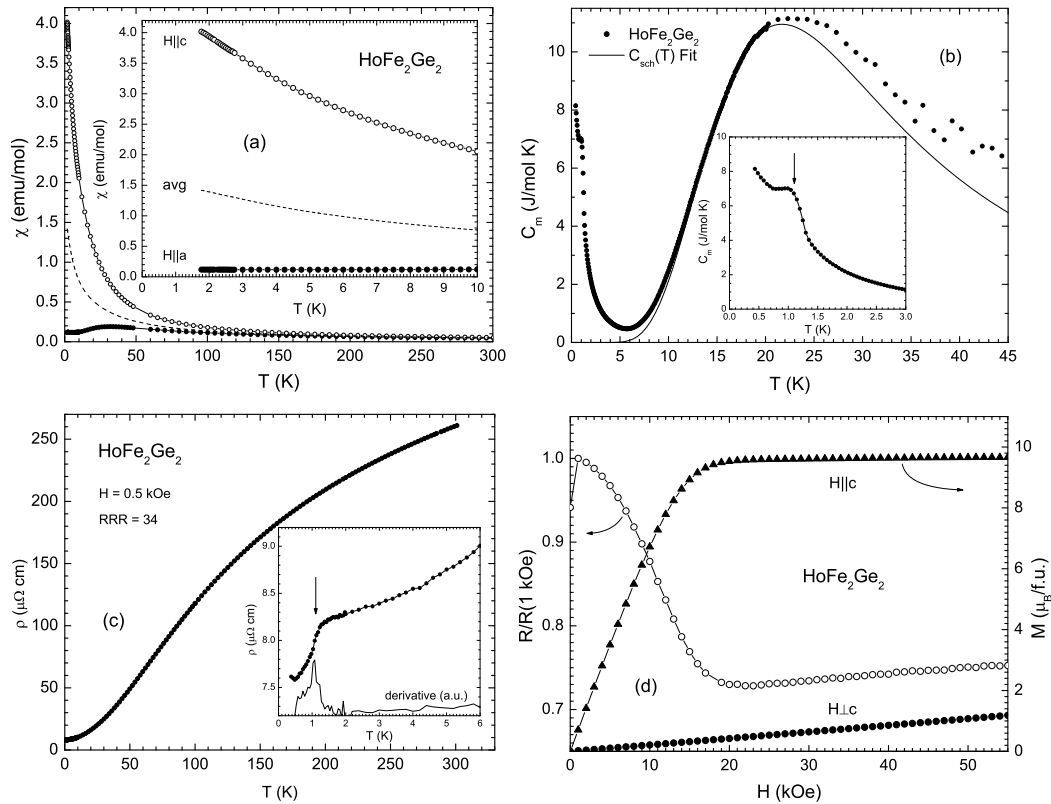


Fig. 10. Measurements on HoFe_2Ge_2 single crystals. (a) Anisotropic susceptibility at $H = 1 \text{ kOe}$ and polycrystalline average. (b) Magnetic heat capacity at $H = 0$ (solid symbols) and fit of eq. 1 (solid line). The inset shows the low temperature region. (c) Resistivity at $H = 0.5 \text{ kOe}$. The inset details the low temperature region (left scale) and $d\rho/dT$ (arbitrary units). (d) Magnetization isotherms at $T = 2 \text{ K}$ (solid symbols) and normalized magnetoresistance (open symbols).

No transitions are observed in our susceptibility measurements on HoFe_2Ge_2 single crystals above 1.8 K (Fig. 10a). The response is very anisotropic, with the axial susceptibility featureless and much greater than in the planar one. $\chi_c(T)$ decreases monotonically, whereas $\chi_a(T)$ shows a local minimum at about 6 K, followed by a broad maximum at about 30 K. Fitting $\chi_c(T)$ above 20 K yields $\chi_{\text{eff}} = 11.0 \mu_B / \text{f.u.}$, slightly above the expected value of $\chi_{\text{eff}} = 10.6 \mu_B / \text{f.u.}$

for Ho^{3+} .

Specific heat measurements of HoFe_2Ge_2 reveal some interesting features (Fig. 10b), and the behavior is in excellent quantitative agreement with that reported by Schobinger-Papamantellos et al. on annealed ingots. A very large Schottky anomaly dominates the low temperature behavior. The dashed line in Fig. 10a represents eq. 1 with $\theta = 66$ K and $g_0 = g_1 = 0.23$. Below 5.6 K $C_m(T)$ begins to rise very sharply again, and a small local maximum close to 1 K can be clearly seen. These features indicate that the heat capacity behavior below 6 K may be a convolution of Ho nuclear Schottky effect with magnetic fluctuations of the electronic moments, including antiferromagnetic ordering of the latter. If this is the case, then the CEF level scheme should consist of a ground state doublet and an 8-fold near-degenerate manifold of CEF levels in the vicinity of $T_{\text{CEF}} \approx 60$ K. The other possible scenario would be that the small peak is not related to magnetic ordering of the Ho moments, and the ground state is a non-magnetic singlet with a 4-fold near-degenerate excited level manifold. The large nuclear Schottky feature prevents a reliable quantitative analysis of the magnetic entropy which would be very useful in distinguishing between these two options, however, we will show below that the first scenario is the more likely one. A simple test of consistency for this hypothesis can be made by ignoring the data below the plateau around 5 K and postulating that the accumulated magnetic entropy up to this temperature has reached $R \ln 2$ due to the antiferromagnetic transition. When this is done (Fig. 9b), the magnetic entropy is seen to approach $R \ln 10$ as the temperature approaches 60 K.

Further corroboration of a magnetically ordered ground state was provided by temperature-dependent resistivity measurements at 0.5 kOe (Fig. 10c), where we can observe a clear loss of spin-disorder scattering below 1.1 K, which we believe is probably associated with an antiferromagnetic transition temperature. It is important to note that the 1.1 K feature is not related in any way to T_N since, by measuring under zero applied field, the small drop due to T_N superconductivity appears at 4 K while the 1.1 K drop remains intact. The high temperature behavior of $\rho(T)$ is similar to all other members, reaching 260 $\mu\Omega$ cm at 300 K, and for this sample $R_{\text{RRR}} = 34$.

Field dependent magnetization at 2 K (therefore above the transition) rises rapidly up to 20 kOe for $H_{\parallel c}$ and remains almost levelled thereafter, reaching $9.7 \mu_B/\text{f.u.}$ at 55 kOe (Fig. 10d). Magnetization in the basal plane is small and perfectly linear with field, reaching $1.19 \mu_B/\text{f.u.}$ at 55 kOe. Magnetoresistance measurements at 2 K show an almost 30% drop which accompanies the field-driven alignment of Ho magnetic moments up to 20 kOe, then assumes a small positive slope up to 90 kOe in the high-field, saturated moments region.

The fact that we observe clear local moment behavior in $M(H)$ at $T = 2$ K indicates that the sample is not in a non-magnetic singlet state with the first

excited CEF states separated by ~ 60 K. The large magnetoresistance at $T = 2$ K also supports this observation. These data support the idea that the 1.1 K transition is magnetic in character, arising from a ground state doublet, and that there is a multiplet of 8 CEF levels at ~ 60 K.

3.9 ErFe_2Ge_2

Except for the determination of its crystal structure and lattice parameters (3), melting temperature (5) and for an early report stating that it is paramagnetic from room temperature down to 4.2 K (24), the properties of ErFe_2Ge_2 have so far remained unexplored.

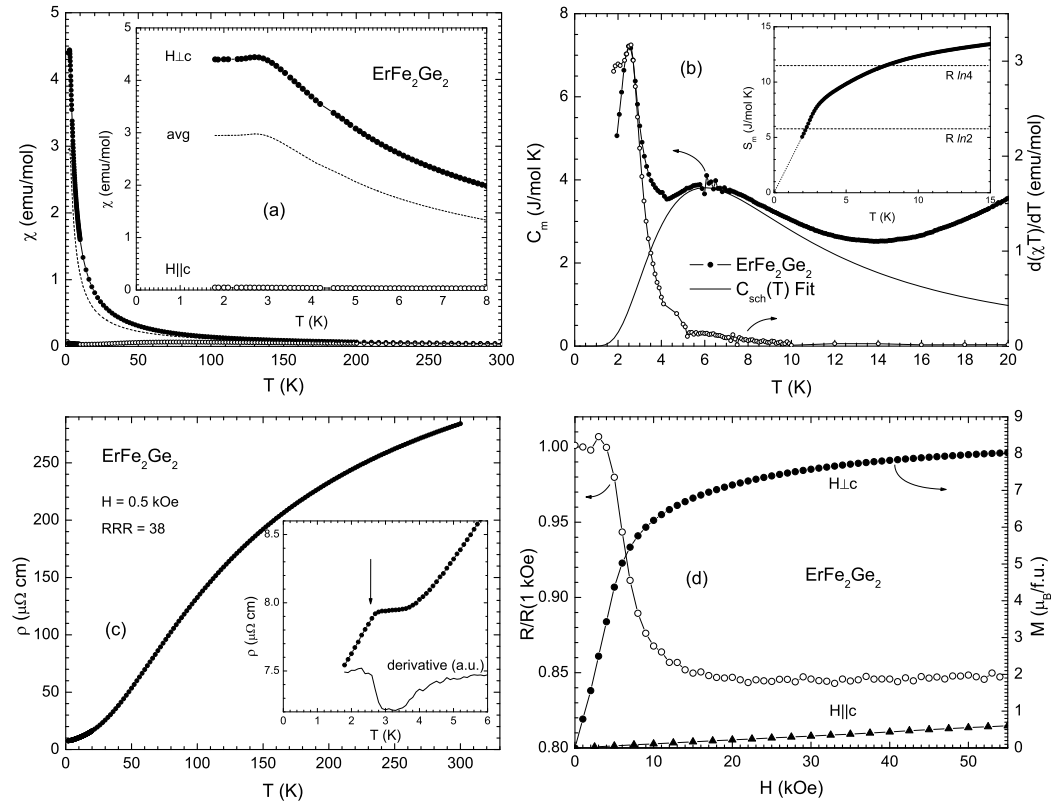


Fig. 11. Measurements on ErFe_2Ge_2 single crystals. (a) Anisotropic susceptibility at $H = 1$ kOe and polycrystalline average. (b) Magnetic heat capacity at $H = 0$ (solid symbols), $d(T)/dT$ from the susceptibility average (open symbols) and fit of eq. 1 (solid line). The inset shows the magnetic entropy, where the dotted line results from integration of the extrapolated $C_m(T)$ data to zero. (c) Resistivity at $H = 0.5$ kOe. The inset details the low temperature region (left scale) and $d(T)/dT$ (arbitrary units). (d) Magnetization isotherms at $T = 2$ K (solid symbols) and normalized magnetoresistance (open symbols).

The magnetic behavior of single crystal ErFe_2Ge_2 is very anisotropic (Fig. 11a), with the moments aligning perpendicular to the c -axis (easy plane), consistent

with a change in sign of the Stevens coefficient B_2^0 in the CEF Hamiltonian (discussed in the following section). $\chi_{ab}(T)$ is large and initially constant between 1.8 and 2.3 K, then rises to a maximum at 2.7 K and drops monotonically up to room temperature. $\chi_c(T)$ is very small, showing a minimum at about 10 K followed by broad maximum at 75 K. Fitting $\chi(T)$ above 20 K yields $\chi_{eff} = 9.5 \mu_B/f.u.$, very close to the free ion value of $9.58 \mu_B/f.u.$ for Er^{3+} . From the peak in $d(\chi(T))/dT$ we estimate $T_N = 2.5$ K (g. 11b).

The magnetic specific heat of $ErFe_2Ge_2$ shows a peak at 2.5 K marking the antiferromagnetic transition, followed by a broad Schottky-like maximum near 6.1 K, above which there still is a significant amount of magnetic entropy probably due to the presence of other CEF levels contributing in this region. The dashed curve in g. 11b is a fit of eq.1, resulting in $\theta = 14.5$ K and $g_0 = g_1 = 0.95$. The scenario seems to be similar to that of $DyFe_2Ge_2$, except for the inverted anisotropy and the rather high values of C_m above the Schottky peak. The magnetic entropy appears to be close to $R \ln 2$ near T_N (inset g. 11b), but the overall behavior doesn't allow a very reliable interpretation probably due to a more complex upper CEF level scheme.

Resistivity for $H = 0.5$ kOe is about $280 \mu\Omega\text{cm}$ at room temperature (g. 11c), decreases like all other members of the series until levelling at about 4 K, then drops again around 2.6 K marking the magnetically ordered state. At 1.8 K the resistivity has been reduced to $7.5 \mu\Omega\text{cm}$, corresponding to $RRR = 38$ which should be taken as a lower limit since the slope is still high at this temperature.

Field dependent magnetization at 2 K and along the ab plane rises very rapidly and initially shows a small upward curvature (g. 11d), which indicates a metamagnetic transition around 3 kOe. By 10 kOe the magnetization is at $6.2 \mu_B/f.u.$ and from there it continues to grow slowly, reaching $8.1 \mu_B/f.u.$ at 55 kOe but still with a positive slope. This may indicate a canted ordering of the moments within the basal plane or in-plane anisotropy, and further investigation of the in-plane magnetic behavior will be required to clarify these issues. The axial magnetization is very small and essentially linear, reaching $0.6 \mu_B/f.u.$ at 55 kOe. Normalized magnetoresistance shows a small peak near 3 kOe, giving support to the existence of a metamagnetic transition, then drops about 15% and remains practically levelled up to 55 kOe.

3.10 $TmFe_2Ge_2$

The magnetic behavior of single crystal $TmFe_2Ge_2$ (g. 12a) is more anisotropic than $ErFe_2Ge_2$, with the moments also aligning perpendicular to the c-axis (easy plane). $\chi_a(T)$ is large and decreases monotonically above 1.8 K,

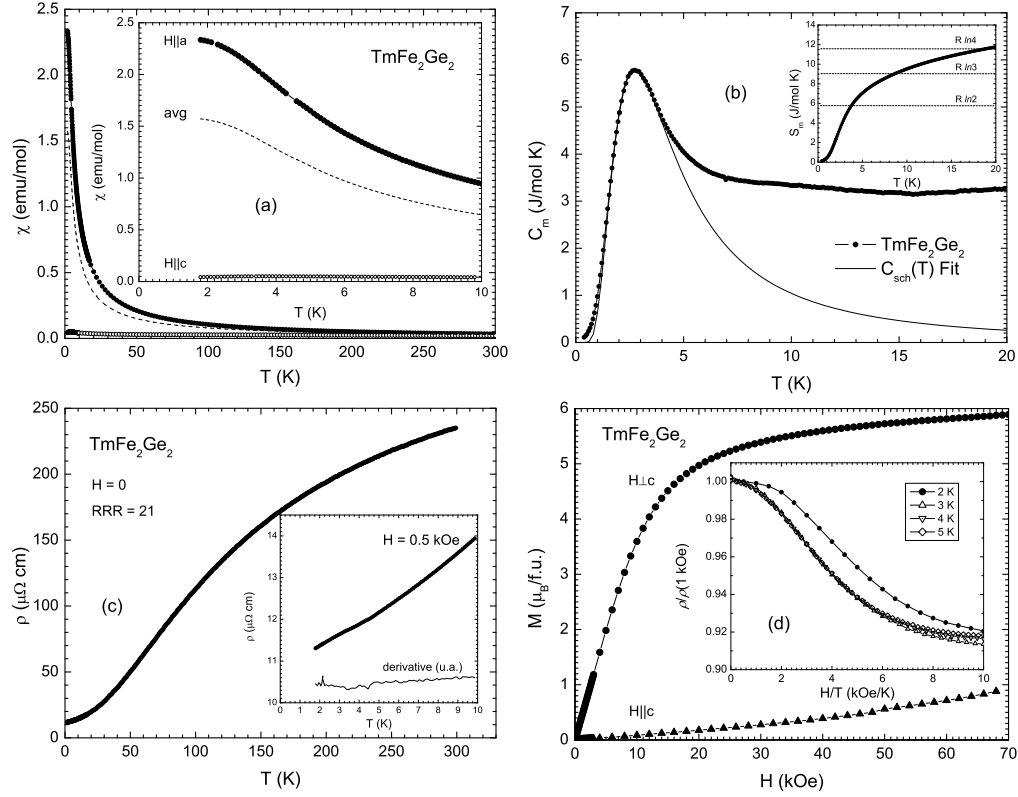


Fig. 12. Measurements on TmFe_2Ge_2 single crystals. (a) Anisotropic susceptibility at $H = 1$ kOe and polycrystalline average. (b) Magnetic heat capacity at $H = 0$ (solid symbols) and fit of eq. 1 (solid line). The inset shows the magnetic entropy. (c) Resistivity at $H = 0$. The inset details the low temperature region (left scale) and $d\rho/dT$ (arbitrary units). (d) Magnetization isotherms at $T = 2$ K. The inset shows normalized magnetoresistance vs: H/T for different temperatures.

although at the lowest temperatures there is a clear change in curvature. $C_m(T)$ is very small and increases to a maximum at 3.8 K, then drops monotonically. It is tempting to attribute this to antiferromagnetic ordering, but the fact that it appeared only in the hard-axis measurement warrants further investigation. As will be shown below, this feature is most likely associated with a crossover to a low temperature non-magnetic singlet ground state. Fitting $C_m(T)$ above 20 K yields $C_{\text{eff}} = 7.8 \text{ B}^2/\text{f.u.}$, slightly larger than the free ion value of $7.56 \text{ B}^2/\text{f.u.}$ for Tm^{3+} .

The specific heat of TmFe_2Ge_2 was measured in the ^3He system to help clarify the sample behavior down to 0.39 K. $C_m(T)$ vs: T shows a large but broadened peak centered at 2.1 K (Fig. 12b), which drops towards zero as the lowest temperatures are reached. The shape is more representative of a Schottky anomaly than a lambda-like ordering peak. Indeed, the lower part fits well to eq. 1 with $\theta = 7.1$ K and $g_0 = g_1 = 0.56$, and the accumulated entropy in this temperature region is close to $R \ln 3$ (inset Fig. 12b). This would be consistent with a non-magnetic CEF singlet ground state and a first excited state

formed by a doublet or two close singlets, allowing the appearance of magnetism by thermal population of these first excited states, but above 7 K the level scheme should have a more complicated distribution of levels (probably mostly singlets with different energy separations) which would require a more elaborate data modelling to fully describe the low temperature behavior. Neglecting these higher states, the obtained level scheme would help explain the curvature observed in $\chi_{ab}(T)$ at the lowest temperatures, since the singlet ground state and energy gap would lead to a levelled van Vleck-like susceptibility for $T \rightarrow 0$. In its simplest modelling (39), the product χ_{vv} , where χ_{vv} is the temperature-independent molar susceptibility, depends only on the non-diagonal matrix element $\langle 0 | j_z | j \rangle$ connecting the singlet ground state 0 with the excited states. If we assume that $\chi_{ab}(T)$ for TmFe_2Ge_2 will level at $\chi_{vv} = 2.4 \text{ emu/mol}$ (g.12a), we obtain $\chi_{vv} = 17 \text{ K emu/mol}$, comparable to 14 K emu/mol that can be estimated for some well known thulium-based van Vleck paramagnets such as TmSb (40) and TmH_2 (41). It should be noted that the expression above is derived for the particular case where the CEF has removed all orbital degeneracies. It is also worth mentioning that in some compounds, strong enough exchange interactions can lead to magnetic ordering even when the CEF ground state is a singlet. For example, TmCu_2Si_2 has been reported (42; 43) as having two singlet states separated by $\Delta = 6.1 \text{ K}$, and yet orders antiferromagnetically at $T_N = 2.8 \text{ K}$. However, such an ordering should be accompanied by a lambda-like peak in the magnetic specific heat as indeed occurs with TmCu_2Si_2 (42), and our measurements show no sign of any such feature down to 0.4 K in TmFe_2Ge_2 .

Zero-field resistivity is about $235 \text{ m}\Omega$ at room temperature (g.12c), and behaves much like LuFe_2Ge_2 upon cooling, showing no clear sign of loss of spin-disorder scattering down to 1.8 K , at which point it is slightly above $11 \text{ m}\Omega$, resulting in $\text{RRR} = 21$.

Field dependent magnetization at 2 K and along the ab plane rises in a reversible Brillouin-like manner (g.12d), reaching only $5.9 \mu_B/\text{f.u.}$ at 70 kOe , lower than the saturated moment of $7 \mu_B/\text{f.u.}$ for Tm^{3+} . The axial magnetization is small and seems essentially linear, although high-field measurements in this orientation were difficult due to the strong torque applied on the sample, arising from $\mathbf{H} \times \mathbf{M}$. Magnetoresistance was measured at $T = 2, 3, 4$ and 5 K . For these temperatures the resistivity is seen to decrease with H rather rapidly until some field value where it reaches a minimum, then assumes a small positive slope. As expected for spin-disorder scattering by paramagnetic moments (44) for $T > T_N$, the normalized resistivity is seen to scale very well with H/T for the measurements between 3 K and 5 K , but not for the measurements at 2 K , indicating that at least some change in the scattering regime of the sample has occurred at 2 K , as a consequence of Tm^{3+} ions dropping into their non-magnetic state.

4 Trends in the series

When crystals are grown in a foreign-element flux it is always good to check whether there is any significant substitution of the phase elements by the flux element. In our case the most likely scenario would be Sn substituting Ge within the structure. If this substitution occurred at a relevant degree, we would expect to see changes in the lattice parameters since Sn is larger than Ge. The refined lattice parameters we obtained from powder x-ray diffractograms on some crushed crystals (figure 13a) are in excellent agreement with published values on arc-melted ingots(3), and further corroboration of phase purity is given by the very low residual resistivities. The general trend of the lattice parameters in this series is consistent with the reduction in size of the rare earth 3+ ion with increasing atomic number, leading to a small decrease of the unit cell volume but also to a small elongation of the tetragonal unit cell. A notable exception is YbFe_2Ge_2 where Yb is reported to be in a mixed or intermediate valency state(45), and this may lead to changes in the phase diagram which resulted in our failure to grow this compound out of Sn flux. Our other failed attempts were for $R = \text{La}$ and Ce due to interference of a secondary cubic phase (probably R_2Sn_3), and EuFe_2Ge_2 which apparently is not a stable phase since there are no reports of successful synthesis of this compound, not even in Felner and Nowik's systematic study of EuT_2Ge_2 arc-melted ingots(33).

Table 1 summarizes the results obtained from our measurements on RFe_2Ge_2 single crystals. For all moment-bearing rare earths (except the spherically symmetric Gd^{3+}), the magnetic behavior of the crystals is extremely anisotropic, with the moments at low temperature confined to either the crystallographic c-axis, or the basal plane. This anisotropy primarily results from the CEF splitting of the Hund's rule multiplet, whose Hamiltonian for a rare earth ion located in tetragonal point symmetry can be written as(47)

$$H_{\text{CEF}} = B_2^0 O_2^0 + B_4^0 O_4^0 + B_4^4 O_4^4 + B_6^0 O_6^0 + B_6^4 O_6^4; \quad (2)$$

where B_n^m are the Stevens coefficients related to the geometrical arrangement of ions surrounding the rare earth, and O_n^m are the Stevens equivalent operators. If the coupling between moments is ignored, at high enough temperatures the CEF anisotropy for tetragonal point symmetry is governed only by the B_2^0 term (48; 49). If the isotropic inverse susceptibility at high temperatures (without CEF splitting) is written as $\chi^{-1}(T) = (T - T_p)/C$, where C is the Curie constant and T_p is the paramagnetic Weiss temperature, then the effect of CEF is to separate $\chi_{ab}^{-1}(T)$ and $\chi_c^{-1}(T)$ by the appearance of orientation-dependent

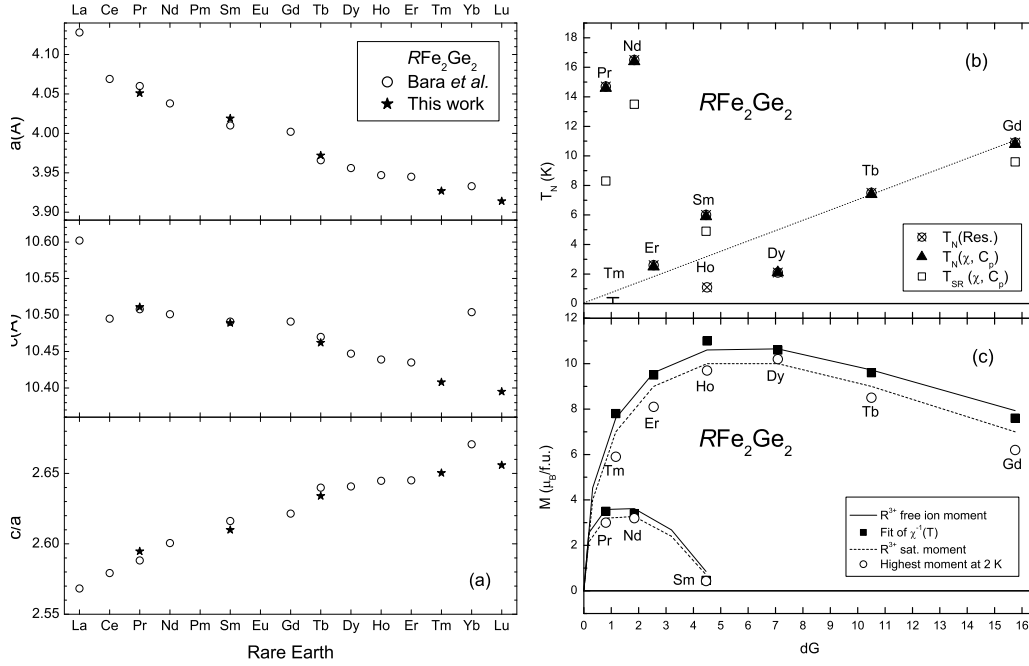


Fig. 13. (a) Lattice parameters obtained from refinements of x-ray powder diffraction patterns on $R\text{Fe}_2\text{Ge}_2$ annealed ingots (Bara et al.(3)) and some selected single crystals (this work). (b) Scaling of the $R\text{Fe}_2\text{Ge}_2$ transition temperatures with de Gennes factor $(g_J - 1)^2 J(J + 1)$. (c) Comparison of the expected and measured values for the free ion moments and saturated moments.

Weiss temperatures θ_{ab} and θ_c , such that(48; 49)

$$(\theta_{ab} - \theta_c) = \frac{3(2J - 1)(2J + 3)}{10} B_2^0; \quad (3)$$

where J is the total angular momentum of the Hund's rule ground state of the rare earth. This expression shows how the magnitude of B_2^0 contributes to the level of anisotropy in the compounds, and the sign of B_2^0 determines whether the compound becomes easy-axis or easy-plane. In the point charge model of CEF we may write

$$B_2^0 = \hbar^2 i A_2^0 \chi_J; \quad (4)$$

where $\hbar^2 i$ is positive by definition, and A_2^0 is a purely geometrical factor which can usually be considered constant throughout a series of rare earth compounds if the changes in lattice parameters are small. It follows that the sign of B_2^0 is governed by the rare earth dependent coefficient χ_J (46), listed in table 1. Note that for the $R\text{Fe}_2\text{Ge}_2$ series $\chi_J < 0$ results in axial moments and $\chi_J > 0$ results in planar moments. Unfortunately we were not able to reliably estimate the Weiss temperatures and their trends, since these are

C om pound	J (10 ²)	E asy orient.	T _N (K)	T _{SR} (K)	0 (em u/m ol)	eff (B)	H F (B)	R R R
Y Fe ₂ G e ₂	–	–	–	–	.0030	–	.038	32
P rFe ₂ G e ₂	–1.05	axial	14.6	8.3	.0053	3.5	3.0	60
N dFe ₂ G e ₂	–.643	axial	16.4	13.5	.0042	3.4	3.2	53
S m Fe ₂ G e ₂	+ 4.13	planar	5.9	4.9	.0039	.46	.43	83
G dFe ₂ G e ₂	–	–	10.8	9.6	.0026	7.6	6.2	68
T bFe ₂ G e ₂	–1.01	axial	7.4	–	.0058	9.6	8.5	32
D yFe ₂ G e ₂	–.635	axial	2.1	–	.0043	10.6	10.2	31
H oFe ₂ G e ₂	–222	axial	1.1	–	.0024	11.0	9.7	34
E rFe ₂ G e ₂	+ .254	planar	2.5	–	.0025	9.5	8.1	38
T m Fe ₂ G e ₂	+ 1.01	planar	< .4	–	.0049	7.8	5.9	21
L uFe ₂ G e ₂	–	–	–	–	.0030	–	.033	23

Table 1

Sum m ary of the m easured properties of the R Fe₂G e₂ single crystals (except J obtained from ref. (46)). T_N = Neel temperature, T_{SR} = second magnetic transition, 0 = temperature-independent susceptibility term, eff = effective moment, H F = highest measured moment at 2 K, R R R = R (300K)=R (1:3K).

obtained from extrapolation of the high temperature behavior of the inverse susceptibility, and in this series the extrapolation is highly sensitive to the non-negligible temperature-independent susceptibility 0 (see table 1), which possibly indicates a large density of states at the Fermi level N (E_F). It is also likely that the coupling between moments is still relevant at intermediate temperatures, so a quantitative study of B₂⁰ trends may also require preparation of crystals for that specific purpose, such as by diluting small fractions of a given moment-bearing rare earth into a non-magnetic isostructural compound (50), e.g. (Y_{1-x}R_x)Fe₂G e₂.

Our measurements made on all antiferromagnetically ordering members empirically demonstrate the equivalence of C_p(T) and d(T)/dT for determining the transition temperatures. The general behavior of d(T)/dT was also very similar, resulting in transition temperatures that were one or two tenths of a degree higher at most. In table 1 we list our best estimates of the transition temperatures obtained from these three techniques. If CEF effects are neglected, the magnetic ordering temperatures T_M across a rare earth series should be describable within the framework of the Weiss molecular field theory, for which we may write (51)

$$T_M = \frac{2}{3} I (g_J - 1)^2 J (J + 1); \quad (5)$$

where I is the exchange interaction parameter and $(g_J - 1)^2 J(J + 1)$ is the de Gennes factor (dG). The latter is representative of the $R-R$ exchange energy, and in cases where the magnetic interaction between the local moments of the rare earth ions occurs indirectly via the conduction electrons (RKKY interaction), the ordering temperatures are expected to follow a linear dependence with dG . Figure 13b shows the Neel temperatures from table 1 plotted against the dG factor. A rough scaling with dG is found for the heavy rare earths (Gd-Er), although significant deviation is seen especially for $R = Dy$ and Ho , indicating a relevant influence of CEF which lowers the ordering temperatures in these compounds.

Estimation of the effective moments in the RFe_2Ge_2 series was far less sensitive to the influence of ρ_0 than the Weiss temperatures. It is worth restating here that the Fe ions are non-magnetic in this series, and the obtained values for μ_{eff} are in good agreement with the expected moments of free rare earth ions in their $3+$ state (Fig. 13c), except for Sm which resulted only about 2/3 of the expected value. This discrepancy in $SmFe_2Ge_2$ is not surprising given its distinct non-Curie-Weiss behavior at high temperatures.

The highest measured moments at 2 K also follow the general trend expected for saturated R^{3+} ions, although except for $R = Dy$ the obtained moments are slightly lower than the expected ones. There are several factors that may be leading to these lower values, the most trivial one being that the highest fields available in our magnetometers (55 and 70 kOe) are insufficient to fully align the moments in some compounds. Other contributing factors may include in-plane anisotropy and/or canted in-plane moments (for the easy-plane members), singlet ground state (Tm), or low-temperature diamagnetic contribution of the itinerant band as described by Duong et al. (30).

The heat capacity measurements were very useful in giving a basic idea of the electronic ground states of most compounds. The non-magnetic members presented an unusually high electronic specific heat contribution ($\sim 60 \text{ mJ/molK}^2$) which very likely persists throughout the entire series and is consistent with the large values found for ρ_0 . Despite the semi-quantitative nature of the analyses leading to calculation of the magnetic entropy (resulting from the need to estimate the non-magnetic contributions and the behavior below our lowest measurable temperatures), it was possible to observe the existence of a ground state doublet for the Kramers ions Nd, Sm, Dy, Er and an octuplet for Gd. Influence of nuclear Schottky effects prevented a definitive quantitative analysis for the non-Kramers ions Pr, Tb and Ho, but good fits of electronic Schottky anomalies also helped infer the lower CEF level schemes of Dy-Tm.

All compounds that ordered above 2 K showed field-driven metamagnetic transitions at that temperature. The transitions were quite sharp for $R = Pr$

and Nd, less so for R = Sm, Gd, Tb, and barely noticeable as a small upward curvature for R = Dy and Er. The differences should be mostly related to the fact that for $T = 2\text{ K}$, $T = T_N$ is 1 for the first group and .1 for the last. The $R\text{Fe}_2\text{Ge}_2$ series does not seem to present cases of intermediate metamagnetic steps at 2 K, but rather a single spin- \uparrow spin- \downarrow transition.

The in-plane resistivity behavior of all crystals in the series behaved very similarly, showing an "s-shaped" curvature up to 300 K which is different from the $R\text{Ni}_2\text{Ge}_2$ series (for example). The similarity of all curves including those for R = Y and Lu indicates that the R ion magnetism is not playing a very significant role in the resistivity behavior above the ordering temperatures, and the lack of any appreciable linear region indicates that standard electron-phonon scattering is not the dominant factor either. It is interesting to note that this "s-shaped" resistivity with anomalously high scattering regimes at medium to high temperatures is frequently observed in materials with high values, such as heavy fermions. The high temperature behavior should also be influenced by the relatively low Debye temperatures $\Theta_D = 280\text{ K}$ and 240 K found for R = Y and Lu respectively. A closer look at the Fermi surfaces of $R\text{Fe}_2\text{Ge}_2$ and how they compare to other $R\text{T}_2\text{Ge}_2$ compounds may provide a better understanding of the role of the Fe ions in these unusual features.

5 Conclusion

In this work we have presented a detailed characterization of $R\text{Fe}_2\text{Ge}_2$ single crystals grown from Sn solution. The high quality of the crystals was attested by residual resistivities and RRR values in the range of 3-12 $\mu\Omega\text{ cm}$ and 20-90 respectively. The crystals are also virtually free of magnetic impurities or secondary phases, allowing the study of the intrinsic anisotropic magnetic behavior of each compound. Strong anisotropies arising primarily from CEF effects were observed for all magnetic rare earths except Gd, leading to moments being confined to either the c-axis or basal plane, as determined by the sign of the Stevens' coefficient B_2^0 . Neel temperatures were determined by three independent techniques, and roughly scale with the de Gennes factor for the heavy rare earths, although for R = Dy and Ho (and possibly Tm) the Neel temperatures have been significantly reduced by CEF effects. A second, lower temperature transition between different magnetic phases was observed for R = Pr, Nd, Sm, and Gd. A single metamagnetic transition at 2 K was found for all members whose moments ordered above 2 K. The calculated effective moments per rare earth atom are close to the expected free ion values of R^{3+} except for Sm which behaves anomalously in the paramagnetic state. Tm was the only moment-bearing rare-earth which did not order down to 0.4 K, and displays anomalously low temperature behavior probably due to a non-magnetic singlet ground state, resulting in a crossover to a Van Vleck-type susceptibility

below 2 K. The non-magnetic members of this series ($R = Y, Lu$) showed an unusually large electronic specific heat coefficient ($\gamma \approx 60 \text{ mJ/mol K}^2$) and temperature-independent susceptibility term ($\chi_0 \approx 0.003 \text{ emu/mol}$), indicative of a relatively large density of states at the Fermi surface. $LuFe_2Ge_2$ was reported for the first time as a compound, and showed a transition at 9 K possibly due to the formation of a charge- or spin-density wave. More detailed investigations of individual compounds in the series, including studies on the in-plane anisotropy, out-of-plane resistivity, neutron diffraction, EPR, ^{57}Fe Mossbauer spectroscopy, and band structure calculations should prove useful in further understanding their individual magnetic and electronic properties. Substitution studies on the Fe and Ge sites may also help understand the peculiarities of the RFe_2Ge_2 compounds compared to other members of the RT_2X_2 family.

We acknowledge the help of R. A. Ribeiro and C. Petrovic in the x-ray diffraction measurements, and K. D. Myers in the early development and characterization of the crystals. We are also thankful to J. Schmalian for fruitful discussions. Ames Laboratory is operated for the US Department of Energy by Iowa State University under Contract No. W-7405-Eng-82. This work was supported by the Director for Energy Research, Office of Basic Energy Sciences.

References

- [1] A. Szytula, J. Leciejewicz, Handbook of Crystal Structures and Magnetic Properties of Rare Earth Intermetallics, CRC Press, 1994, pp. 114-171.
- [2] D. Rossi, R. Marazza, R. Ferro, J. Less-Common Met. 58 (1978) 203.
- [3] J. J. Bara, H. U. Hryniewicz, A. Mils, A. Szytula, J. Less-Common Met. 161 (1990) 185.
- [4] G. Venturini, B. Malaman, J. Alloys Compds. 235 (1996) 201.
- [5] A. V. Morozkin, Y. D. Seroegin, A. V. Gribanov, J. M. Barakatova, J. Alloys Compds. 256 (1997) 175.
- [6] A. V. Morozkin, Y. D. Seroegin, A. V. Gribanov, I. A. Sviridov, J. M. Kurenbaeva, A. L. Kurenbaev, J. Alloys Compds. 264 (1998) 190.
- [7] I. Felner, I. Mayer, A. Grill, M. Schieber, Solid State Commun. 16 (1975) 1005.
- [8] T. Ebihara, K. Motoki, H. Toshima, M. Takashita, N. Kimura, H. Sugawara, K. Ichihashi, R. Settai, Y. Onuki, Y. Aoki, H. Sato, Physica B 206-207 (1995) 219.
- [9] H. Sugawara, Y. Aoki, H. Sato, N. Moshnikov, S. Hane, T. Goto, J. Phys. Soc. Jap. 68 (1999) 1094.
- [10] H. Sugawara, T. Namiki, S. Yuasa, T. D. Matsuda, Y. Aoki, H. Sato, N. Moshnikov, S. Hane, T. Goto, Physica B 281-282 (1999) 69.

- [11] R. A. Neifeid, M. Croft, T. Mihalisin, C. U. Segre, M. Madigan, M. S. Torikachvili, M. B. Maple, L. E. DeLong, Phys. Rev. B 32 (1985) 6928.
- [12] P. H. Ansari, B. Qi, G. Liang, I. Perez, F. Lu, M. Croft, J. Appl. Phys. 63 (1988) 3503.
- [13] S. L. Bud'ko, M. B. Fontes, G. H. Walf, D. Mienert, E. M. Baggio-Saitovitch, Mater. Sci. Forum 302-303 (1999) 375.
- [14] Z. Fisk, J. P. Remeka, in Handbook on the Physics and Chemistry of Rare Earths, Vol. 12, Elsevier, Amsterdam, 1989.
- [15] P. C. Canfield, Z. Fisk, Phil. Mag. B 65 (1992) 1117.
- [16] P. C. Canfield, I. R. Fisher, J. Crystal Growth 225 (2001) 155.
- [17] M. E. Fisher, Phil. Mag. 7 (1962) 1731.
- [18] B. Malaman, G. Venturini, A. Blaise, J. P. Sanchez, G. Amoretti, Phys. Rev. B 47 (1993) 8681.
- [19] M. E. Fisher, J. S. Langer, Phys. Rev. Lett. 20 (1968) 665.
- [20] M. Escome, A. Mauger, D. Ravot, J. C. Achard, J. Phys. C 14 (1981) 1821.
- [21] T. A. Wiener, I. R. Fisher, S. L. Bud'ko, A. Kricher, P. C. Canfield, Phys. Rev. B 62 (2000) 15056.
- [22] S. L. Bud'ko, Z. Islam, T. A. Wiener, I. R. Fisher, A. H. Lacerda, P. C. Canfield, J. Magn. Magn. Mater. 205 (1999) 53.
- [23] R. S. Kwok, S. E. Brown, Phys. Rev. Lett. 63 (1989) 895.
- [24] S. K. Malik, S. G. Sankar, V. U. S. Rao, R. Obermeyer, AIP Conference Proceedings 29 (1976) 585.
- [25] J. Leciejewicz, A. Szytula, A. Zygmunt, Solid State Commun. 45 (1983) 149.
- [26] A. Szytula, W. Bazela, J. Leciejewicz, J. Phys. Chem. Solids 48 (1978) 1053.
- [27] A. Szytula, A. Oles, M. Perrin, J. Magn. Magn. Mater. 86 (1990) 377.
- [28] A. Blaise, B. Fak, J. P. Sanchez, G. Amoretti, P. Santini, R. Caciuto, D. Schm itt, B. Malaman, G. Venturini, J. Phys. Condens. Matter 7 (1995) 8317.
- [29] V. Ivanov, L. Vinokurova, A. Szytula, A. Zygmunt, J. Magn. Magn. Mater. 114 (1992) L225.
- [30] N. P. Duong, E. Bnick, P. E. Brommer, J. C. P. Klaase, F. R. de Boer, K. H. J. Buschow, J. Magn. Magn. Mater. 242-245 (2002) 813.
- [31] N. P. Duong, K. H. J. Buschow, E. Bnick, J. C. P. Klaase, P. E. Brommer, L. T. Tai, T. D. Hien, J. Alloys Compds. 298 (2000) 18.
- [32] F. M. Mulder, R. C. Thiel, K. H. J. Buschow, J. Alloys Compds. 202 (1993) 29.
- [33] I. Felner, I. Nowik, J. Phys. Chem. Solids 39 (1978) 767.
- [34] P. C. Canfield, J. D. Thompson, W. P. Beyermann, A. Lacerda, M. F. Hundley, E. Peterson, Z. Fisk, H. R. Ott, J. Appl. Phys. 70 (1991) 5800.
- [35] M. Bouvier, P. Lethuillier, D. Schm itt, Phys. Rev. B 43 (1991) 13137.
- [36] H. Pinto, M. Melamed, M. Kuznietz, H. Shaked, Phys. Rev. B 31 (1985) 508.

- [37] W .Bazela, J.Leciejewicz, H .Ptasiewicz-Bak, A .Szytula, J.Magn.Magn. Mater. 72 (1988) 85.
- [38] A .Szytula, S. Baran, J. Leciejewicz, B .Penc, N .Stusser, Y .F. Ding, A .Zygmunt, J. Zukrowski, J. Phys. Condens. Matter 9 (1997) 6781.
- [39] C. Kittel, Introduction to Solid State Physics, 4th Edition, John Wiley and Sons, USA .
- [40] C. Rettori, D. Davidov, A .Grayevsky, W .M .Walsh, Phys. Rev. B 11 (1975) 4450.
- [41] H .Weizenecker, H .Winter, H .J. Mattausch, E .Dormann, J. Magn. Mater. 152 (1996) 183.
- [42] G .A .Stewart, J. Zukrowski, A .Kozłowski, Hyper ne Interactions 40 (1988) 433.
- [43] M .Kosaka, H .Onodera, K .Ohoyama, M .Ohashi, Y .Yamaguchi, S. Nakamura, T .Goto, J. Phys. Soc. Jpn. 66 (1997) 2844.
- [44] I. R. Fisher, J. R. Cooper, P. C. Can eld, Phys. Rev. B 56 (1997) 10820.
- [45] M .N. Groshev, M .D. Koterlin, E .M .Levin, R .V. Lutsiv, N .M .Miftakov, Y .P. Smimov, A .E. Sovestnov, A .V. Tyunis, V .A .Shubarov, Fiz. Tverd. Tela 28 (1986) 2711.
- [46] M .T. Hutchings, in Advances in Research and Applications, Solid State Physics, Vol. 16, Academic Press, New York, 1964.
- [47] J. L. P rather, U .S. International Bureau of Standards Monograph No. 19.
- [48] Y .L. Wang, Phys. Lett. A 35 (1971) 383.
- [49] P. Boutron, Phys. Rev. B 7 (1973) 3226.
- [50] B. K .Cho, B .N. Harmon, D .C .Johnston, P. C .Can eld, Phys. Rev. B 53 (1996) 2217.
- [51] D .R. Noakes, G .K .Shenoy, Phys. Lett. A 91 (1982) 35.